Journal of Medicinal Chemistry

pubs.acs.org/jmc

Article

Discovery of a Pyrazolopyridinone-Based MYC Inhibitor That Selectively Engages Intracellular c-MYC and Disrupts MYC−MAX Heterodimerization

Oluwatosin A. Obisesan, Samuel Ofori, Owamagbe N. Orobator, Himanshi Sharma, Emma Groetecke, and Samuel G. Awuah*

Cite This: *J. Med. Chem.* 2025, 68, 6233−6251

Read Online

ACCESS | Metrics & More | Article Recommendations | Supporting Information

ABSTRACT: c-MYC is an oncogenic transcription factor that plays a crucial role in the regulation of downstream targets involved in proliferation, apoptosis, differentiation, metabolism, signaling, and immune response processes whose deregulation leads to the progression of different pathologies. The development of selective and potent small-molecule inhibitors of c-MYC remains a grand challenge in chemical biology and medicine due to its undruggability, derived from extensive intrinsic disorder. In this study, we identified a novel dihydro pyrazolo pyridinone scaffold, **MY05**, that selectively targets c-MYC in cells and disrupts MYC−MAX interaction. MY05 engages intracellular c-MYC, modulates c-MYC thermal stability, reduces c-MYC transcriptional targets, and inhibits proliferation in cancer cells and tumor growth in mice. In summary, we identified a novel compound that directly interacts with c-MYC to disrupt the transcriptional program.

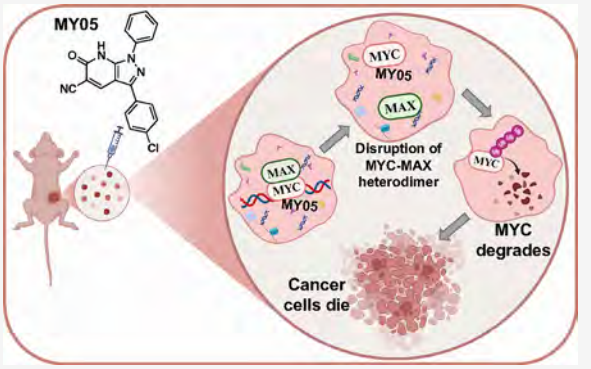

INTRODUCTION

The MYC family of proteins has long been identified as key regulators of cellular processes crucial to both the physiology and implicated in the pathology of humans.[1] As transcription factors, these proteins regulate the formation of gene products important for cell proliferation and differentiation, progression of the cell cycle, apoptosis, metabolism, signaling, and immune responses.[2−4] In normal physiology, cells are found to express low levels of MYC, with an increase in MYC levels observed during active proliferation.[5] However, MYC expression and activities are tightly regulated to ensure the controlled proliferation of cells.[6] In the event of overexpression, deregulation, translocation of the MYC gene, impaired turnover,[7] or the less commonly implicated mutation,[8] c-MYC (commonly and hereafter referred to as MYC), L-MYC, and N-MYC have been associated with the development and progression of the majority of human cancers.[9] Increasing evidence now links the deregulation of MYC to other pathologies, including inflammation and heart diseases.[10,11]

MYC, an intrinsically disordered protein, belongs to a class of basic helix−loop−helix leucine zipper (b-HLH-LZ) proteins. Structurally, MYC consists of an N-terminal transcription activation domain with which it recruits other transcription activators, a central domain comprising conserved sequences like usually unstructured Myc boxes I and II[12,13] and a C-terminal basic helix−loop−helix domain.[14,15] MYC heterodimerizes with MAX using its C-terminal basic helix−loop−helix domain to form a domain that interacts specifically with the enhancer box of the DNA,[16] subsequently recruits other proteins,[17] and ultimately elicits its role of gene transcription. On its own, MYC has weak binding to the DNA,[18] which makes its heterodimerization with MAX a crucial cellular event for its transcriptional activity[19] and the disruption of this heterodimerization a therapeutic window in MYC-driven disease conditions.

The clinical relevance of the role of MYC in diseases such as cancer is unequivocal, considering the extensive studies and correlation between MYC levels and aggressively proliferating tumors.[20−23] MYC is hence an attractive therapeutic target, and it targets an unmet medical need.[24−28] Direct targeting of MYC using small molecules is an approach that is being explored by many in the treatment of various cancers, but several of these attempts to target MYC intracellularly have been terminated prematurely due to the structural dynamics of the protein.[9,29−38] The lack of a deep hydrophobic pocket for the binding of drug molecules has limited the development of

Received: October 21, 2024
Revised: February 17, 2025
Accepted: March 5, 2025
Published: March 13, 2025

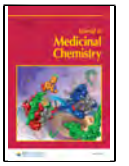

https://doi.org/10.1021/acs.jmedchem.4c02556
J. Med. Chem. 2025, 68, 6233−6251

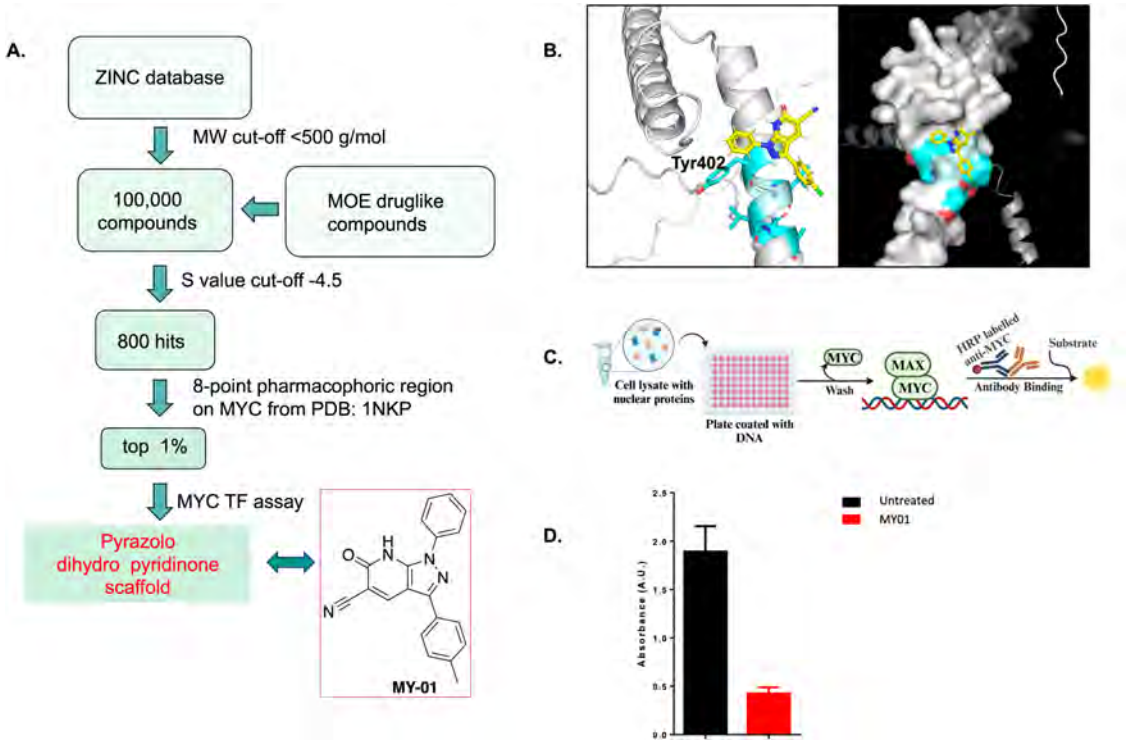

Figure 1. Discovery of novel MYC inhibitors. (A) Flowchart of *in silico* studies for the identification of pyrazole-based MYC inhibitors. (B) Docking-generated binding pose showing interactions between the MYC inhibitor and amino acid residues of the full MYC protein (AFDB: AF-P01106-F1-v4) at the b-HLH-LZ domain. (C) Illustration of the transcription factor (TF) activity assay and (D) bar chart showing inhibition of active MYC by MY01 determined by the transcription factor activity assay.

inhibitors that engage MYC for its regulation. Poor nuclear permeability, lack of specificity, and selectivity of potential therapeutic agents have also contributed to stunted advancement of some developed small molecules to the clinic.[39] Maintaining a balance between potency and selectivity has been the major setback for most potential MYC inhibitors.[40,41] Despite the challenges in directly targeting MYC, success in the development of an MYC peptidomimetic, Omomyc in selective regulation of MYC's activities *in vivo* has shown that this seemingly "undruggable" protein can be targeted after all.[5,39,42−44] There is, however, still an urgent need for efficacious and selective small-molecule inhibitors of MYC for the treatment of cancers in the clinic.

While largely disordered, targeting structured hotspots of MYC, particularly regions crucial for the dimerization with MAX, has shown significant progress in the discovery efforts of MYC inhibitors.[38,45,46] We previously reported a covalent inhibitor of MYC, developed based on an in-house transition-metal-based "metal-mediated ligand affinity chemistry (MLAC)"[47] strategy using 10058-F4 as an affinity ligand. The established affinity of 10058-F4 for MYC and the resultant disruption of MYC−MAX heterodimerization point toward the therapeutic potential of the discovery of chemotypes targeting the basic helix−loop−helix hotspot.[34,48] Here, we report the hotspot-targeted discovery and development of novel pyrazole-based compounds that could serve as affinity ligands of MYC. By expanding the library of affinity ligands of MYC with good selectivity and potency, we can advance the discovery of small molecules possessing chemical groups that can be easily functionalized for potent targeting and regulation of MYC intracellularly.

RESULTS

Identification of Pyrazole-Based MYC Inhibitors. The discovery of novel scaffolds that engage MYC is crucial to identifying potent small-molecule inhibitors of this seemingly undruggable protein. Our rational approach as illustrated in Figure 1A started with the *in silico* screening of chemically diverse druglike compounds from the ZINC[49] and Molecular Operating Environment (MOE) databases.[50] Of note, we utilized the MOE molecular docking platform for all *in silico* studies reported herein. Based on previously developed and extensively characterized inhibitor of MYC in our lab, which was premised on the prototypical 10058-F4[34] as an affinity ligand to which a gold warhead was attached for covalent engagement of intracellular MYC,[48] we hypothesized that the MYC402-412 binding region will be a suitable target to expand the MYC chemical space. MYC402-412 region is in the b-HLH-LZ domain of MYC, which is a bonafide structural region necessary for heterodimerization with MAX as well as binding to the E-box consensus sequence of DNA for transcription.[51] Therefore, engaging this domain is crucial for MYC modulation and consequently MYC-related transcriptional activity. In this work, we rationalized that novel chemical agents that disrupt MYC−MAX via the MYC402-412 region will significantly compromise the MYC transcriptional program and act as tool compounds or potential therapeutics in MYC biology or cancer, respectively. Following the compilation of 100,000 druglike small-molecule compounds that were PAINS-filtered and possessed a molecular weight cutoff of 500 g/mol from the ZINC and MOE databases, the compounds were docked against MYC. The *S* value of −4.5 kcal/mol was set as the cutoff to select 800 hit compounds for further validation using the 8-point pharmacophoric region on MYC using the

https://doi.org/10.1021/acs.jmedchem.4c02556
J. Med. Chem. 2025, 68, 6233−6251

Scheme 1. Synthesis of Compounds MY01−MY07

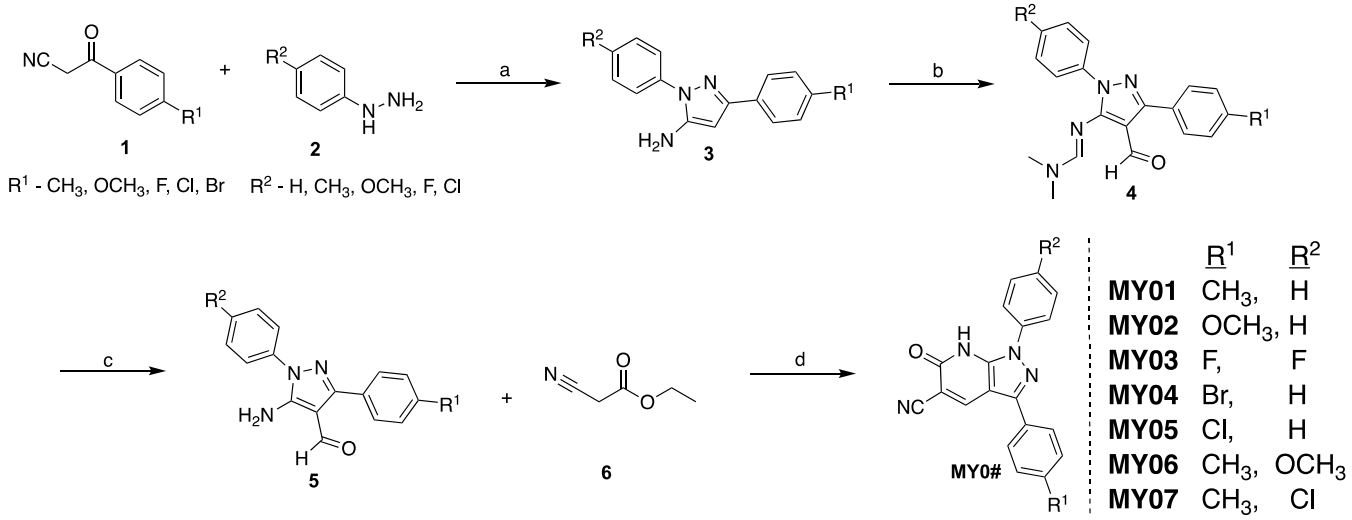

[a]Cat. HCl, EtOH, reflux, 12 h (>86% yield). [b]DMF, $POCl_3$, 75 °C, 5 h (>90% yield). [c]NaOH (aq), EtOH, 75 °C, 3 h (>80% yield). [d]Piperidine, EtOH, reflux, 5 h (30−67% yield).

Chart 1. Structures of Pyrazole-Based Compounds in the MY Series

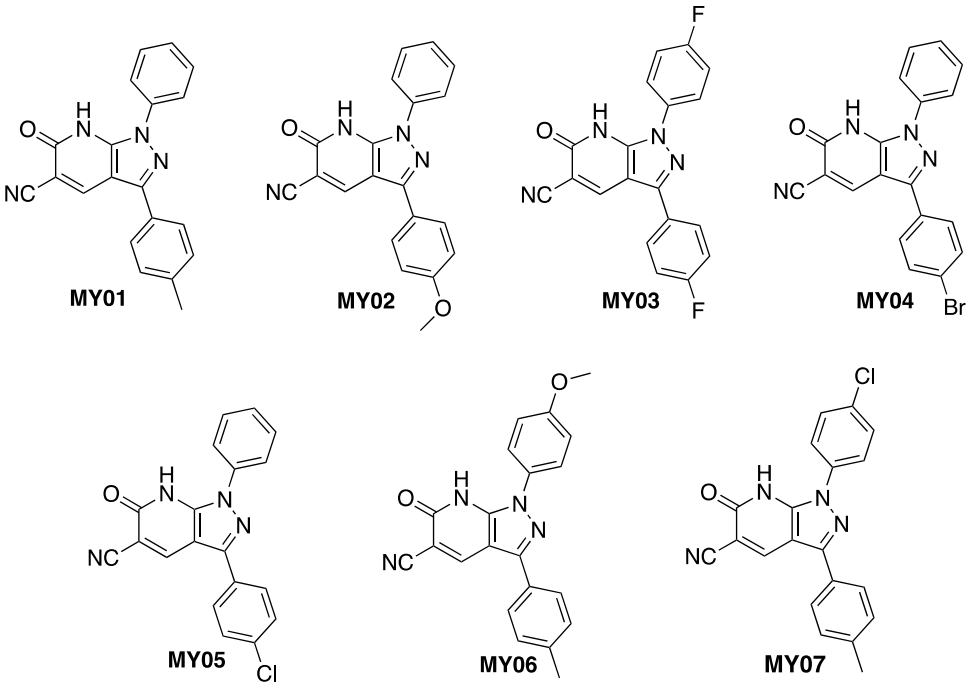

crystal structure from PDB: 1NKP and validated with a full MYC alphafold structure, AFDB: AF-P01106-F1-v4 (Figure 1A,B).[52−54] Subsequently, 8 compounds representing 1% of the overall identified hits were subjected to a preliminary cell-based MYC transcription factor activity assay to identify MY01, a pyrazolo dihydro pyridinone scaffold (Figure 1C,D). Throughout the high throughput *in silico* campaign, reported MYC inhibitors, 10058-F4 and Mycro2;[34,55] were used as reference and dummy compounds.

MY01 interacts with MYC402-409 via a pi-stacking interaction with the Tyr402 of MYC, which was consistent with reported studies of 10058-F4's formation of a "hydrophobic cluster" with the Tyr402 of MYC.[33,56−59] This interaction with an amino acid of MYC gave an indication of potential inhibition of transcriptional activity and possible disruption of MYC−MAX dimerization by our identified chemotype.[60] Other identified hydrophobic interactions and hydrogen bonding further substantiated the hit as a desirable MYC target. Further, we proceeded to diversify MY01 via a streamlined structure−activity relationship (SAR) study.

As shown in Scheme 1, the synthesis of **MY01−07** proceeded via an acid-catalyzed reaction of substituted benzoyl acetonitrile (**1**) with substituted phenyl hydrazine (**2**) under refluxing conditions in ethanol to afford a tan-colored phenyl pyrazole powder after recrystallization from ethyl acetate. Formylation of (**3**) using standard phosphorus oxychloride and *N*,*N*-dimethylformamide (DMF)-generated compound **4** with the installed aldehyde on the pyrazole core, whereas it formed

https://doi.org/10.1021/acs.jmedchem.4c02556
J. Med. Chem. 2025, 68, 6233−6251

dimethylamino imine on the amine functionality adjacent to the aldehyde group. Subsequent base hydrolysis using sodium hydroxide led to the removal of the imine to restore the free amino group, setting the stage for cyclization with ethyl 2-cyanoacetate. This reaction proceeded in the presence of piperidine in ethanol under reflux conditions to form a pyrazolo dihydro pyridinone (**MY01−07**) class of compounds (Chart 1). The different substituents found on the phenyl rings pendant to the pyrazole convey different electronic, steric, and physicochemical properties that impact MYC selectivity and cell viability.

Antiproliferative Activity of the MY Class of Compounds. To examine the anticancer activity of the pyrazolo dihydro pyridinone (**MY01−07**) class of compounds, preliminary cell viability studies across three MYC-driven breast cancer cell lines, namely, MDA-MB 231, MDA-MB 468, and MCF-7, were performed using the 3-(4,5-dimethylthiazol-2-yl)-2,5-diphenyltetrazolium bromide (MTT) assay. Briefly, adhered cells were treated with a wide 8-point concentration range of **MY01−07** or 10058-F4, which is a well-established MYC−MAX disruptor,[61] after which the colorimetric MTT assay was performed. The data suggest that MY04, MY05, and MY06 display superior potency across all cell lines (Table 1),

Table 1. Cell Viability of MY01−07 Represented as IC_{50} (μM) in Breast Cancer Cell Lines MDA-MB 231, MDA-MB 468, and MCF-7 after Exposure for 96 h[a]

	MDA-MB 231	MDA-MB 468	MCF-7
10058-F4	44.7 ± 0.11	39.8 ± 0.10	ND
MY01	34.7 ± 0.10	32.4 ± 0.20	20.4 ± 0.03
MY02	38.0 ± 0.03	33.1 ± 0.08	16.6 ± 0.02
MY03	>100	79.4 ± 0.07	9.3 ± 0.03
MY04	5.5 ± 0.07	13.2 ± 0.06	12.2 ± 0.03
MY05	10.6 ± 0.02	13.5 ± 0.11	39.4 ± 0.03
MY06	9.8 ± 0.02	7.9 ± 0.07	9.3 ± 0.04
MY07	58.9 ± 0.11	71.6 ± 0.17	>100

[a]All compounds were freshly prepared in DMSO and used immediately. DMSO concentration was <1%. ND − not determined.

with IC_{50} values within 5−14 μM in most cell lines investigated. These compounds showed great promise as potent inhibitors of cell proliferation in the MYC-driven cancer cell lines tested.[62,63] The result indicates the structure−function relationship in the context of cell viability and contributes to compound prioritization efforts as less potent compounds may be eliminated from selectivity studies performed in this report (*vide infra*).

Furthermore, MYC selectivity studies were conducted in cells to verify whether the compounds induced antiproliferative activity by targeting the MYC protein. The human lymphoblastoid cell line with inducible MYC expression under the control of tetracycline affords isogenic cell lines with different MYC protein expression levels that enable selectivity studies to be performed in an unbiased fashion.[64,65] By leveraging modulated MYC expression in the same cell line with tetracycline and estradiol treatment,[66] we determined the potency and selectivity of the selected MY class of compounds for MYC. Of note, wild-type P493-6 cells express abundant MYC (MYC^{ON}), whereas P493-6 cells treated with 0.1 μg/mL tetracycline for 72 h shut down MYC expression in cells (MYC^{OFF}), and a combination of 0.1 μg/mL tetracycline and 1 μM estradiol treatment gives low MYC expression (MYC^{LOW}). First, we verified MYC expression levels by fluorescence-activated cell sorting (FACS) analysis, as shown by the forward side scatter gating based on cell size and granularity depicted in Figure 2A. This was further confirmed by western blot to evaluate MYC protein expression, as shown in Figure 2B. Second, with the validated cell models in hand, P493-6-MYC^{ON} with the high expression of MYC and P493-6-MYC^{OFF} cell expression were exposed to 10058-F4 or MY01−06 for 96 h followed by the Cell Titer Glo assay with the exception of MY07 due to lack of sufficient potency in MYC-dependent breast cancer cells (Figure 2C). MY02, MY04, and MY05 had the best selectivity index of all tested compounds. Strikingly, MY02 was most selective for MYC with a 4-fold selectivity index at an IC_{50} of 20 μM in P493-6-MYC^{ON} and >100 μM in P493-6-MYC^{OFF} cells. However, MY02 had a comparatively lower potency in MYC-dependent breast cancer cell lines. Despite the high potency of MY04 in the preliminary MTT assays in breast cancer cell lines, its selectivity index was 2.3-fold, whereas MY05 had an appreciable selectivity index of 3.9. We observed that MY01, MY03, and MY06 had reduced potency and MYC selectivity. The MYC−MAX disruptor 10058-F4 was used as a positive control for the selectivity studies and had an SI of 1.7. On balance, the superior potency and selectivity of MY05 made it an attractive candidate for prioritization and further testing. In an independent study that evaluated the potency and selectivity of MY04 or MY05 at 25 μM on P493-6-MYC^{OFF} or P493-6-MYC^{ON} cells (Figure 2D,E), we found that MY04 and MY05 were significantly selective for MYC-expressing cells compared to MYC-nonexpressing cells.

Considerations of MY05-Induced MYC Conformations in Solution. The intrinsic disorder and helical character of a truncated MYC protein (12 kDa) bearing the pharmacophore region for MY05 or 10058-F4 were expressed and examined by circular dichroism (CD). Consistent with the reports by Hammoudeh et al. and Metallo et al.[33,36,59] the MYC protein has conserved intrinsic disorder (204−208 nm) as well as helicity (220−222 nm), respectively. Using a meta-predictor of the intrinsically disordered region (PONDR),[67] Tyr402, with which our chemotypes interact, was confirmed to be in the ordered region of the protein (Figure 3A). Although CD studies alone are incapable of ascribing disorder and/or helicity to monomeric or dimerized MYC in solution, an understanding of conformational changes induced by MY05 can be gleaned. A mixture of MYC and MY05 in buffer (pH 8) at room temperature showed peak suppression around the 208 nm region (Figure 3B), often assigned to the intrinsic disorder with no major changes to the helical region of MYC.[33] This result is consistent with the reported literature regarding 10058-F4 or 10074-G5 with MYC peptides.[33] The effect of MY05 on the truncated MYC protein under elevated thermal conditions was assessed by thermal denaturation CD from 23 to 70 °C (Figure 3C,D). Given that the change of a protein or polypeptide as a function of temperature may be a result of folding or unfolding transitions,[68] the minimal change in the ellipticity of MYC incubated with MY05 at 208 nm as a function of temperature is suggestive of an induced folded or unfolded protein conformation, whereas free MYC likely undergoes unfolding as a function of temperature.[69] In the helical region, a slightly pronounced folding−unfolding transition is observed for MYC incubated with MY05 compared to that for free MYC based on the change in ellipticity as a function of temperature. Subsequently, the

https://doi.org/10.1021/acs.jmedchem.4c02556
J. Med. Chem. 2025, 68, 6233−6251

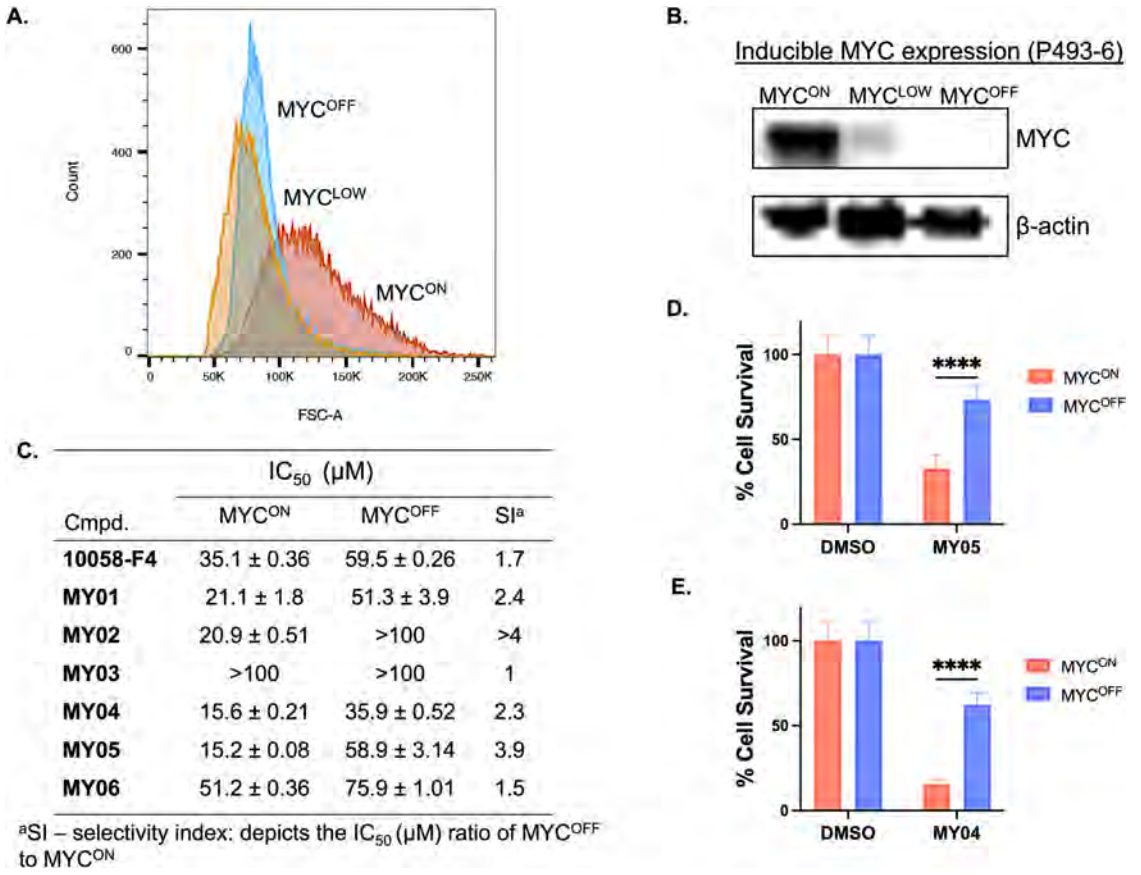

C.

Cmpd.	IC_{50} (μM) MYC^{ON}	MYC^{OFF}	SI[a]
10058-F4	35.1 ± 0.36	59.5 ± 0.26	1.7
MY01	21.1 ± 1.8	51.3 ± 3.9	2.4
MY02	20.9 ± 0.51	>100	>4
MY03	>100	>100	1
MY04	15.6 ± 0.21	35.9 ± 0.52	2.3
MY05	15.2 ± 0.08	58.9 ± 3.14	3.9
MY06	51.2 ± 0.36	75.9 ± 1.01	1.5

[a]SI – selectivity index: depicts the IC_{50} (μM) ratio of MYC^{OFF} to MYC^{ON}

Figure 2. *In vitro* screening of MYC inhibitors for MYC selectivity in P493-6. (A) Overlay of a histogram showing cell sizes of P493-6 cells treated with 0.1 μg/mL tetracycline to turn off MYC expression (blue), a combination of 0.1 μg/mL tetracycline, and 1 μM estradiol for low MYC expression (yellow), or untreated with high MYC expression (red) obtained by flow cytometry and confirmed by western blot in (B). (C) Table comparing IC_{50} (μM) values of inhibitors in P493-6 cells expressing high and no MYC after 96 h treatment. (D) Quantified % cell survival of P493-6 cells treated with MY05 and MY04 (E) at 25 μM treatment for 96 h. Data represented as mean ± standard deviation (SD), $n = 6$, and analyzed by unpaired Student's *t*-test (****$p < 0.0001$).

change in the ellipticity of MYC at 208 nm as a function of concentration was only prominent at a high concentration of 100 μM (Figure 3E).

Thermal stability and ligand interaction can be monitored by a thermal denaturation assay using fluorescent dyes known as the thermal shift assay.[70] Capitalizing on the common effect of protein stabilization or destabilization by ligands,[71] we sought to understand the nature of interactions between MY05 and the recombinant truncated MYC protein used for CD studies (vide supra). Incubation of MYC and MY05 (25 μM) showed a reduced melting temperature of 35 °C compared to MYC alone at 39 °C, indicative of protein destabilization (Figure 3F,G). We posit that MY05 interacts with MYC to induce protein destabilization.

MY05 Engages Intracellular MYC. Intracellular MYC target engagement by MY05 was investigated by the cellular thermal shift assay (CETSA),[72] which is used to assess thermally induced unfolding to provide melting curves for a protein. These melting curves typically shift to a higher temperature when a ligand binds and stabilizes the protein target.[73] However, the opposite destabilization effect of ligands on proteins can be observed.[74] The impact of MY05 on endogenous MYC was conducted by treating P493-6 cells with MY05 (25 μM) or not for 2 h, collected, followed by heating at 30, 34, 38, 42, 46, 50, 54, and 58 °C to denature and precipitate MYC protein, cell lysis, removal of cell debris and aggregates by centrifugation, and final detection of soluble MYC using a specific antibody by immunoblotting. The MYC aggregation temperatures without MY05 were determined to be 42−46 °C, but MYC with MY05 shifted to reduced temperatures at 38−42 °C, suggesting that MY05 destabilizes the intracellular MYC protein (Figure 4A). In an isothermal dose−response assay at 42 °C, MY05 induces thermal destabilization of MYC from 10 to 50 μM (Figure 4B,C).

To further study MY05's interaction with intracellular MYC, we performed immunoprecipitation of MYC in the presence of MY05 and monitored the effect on coimmunoprecipitated MAX by western blot. In both P493-6 and MDA-MB-468 cells, there was a noticeable depletion of coimmunoprecipitated MAX from 3 to 12 h (Figure 4D,E). This has implications for MYC−MAX disruption by MY05, leading to degradation of MYC. In all stages of the experiment, MAX input was measured to calibrate the amount of MAX in the lysates used. The disruption of MYC−MAX heterodimerization intracellularly was further confirmed in MDA-MB 468 cells by the proximity ligation assay (PLA), which is an immunofluorescence-based assay premised on the production of fluorescence signals formed when MYC and MAX are in proximity, as they would be when heterodimerized (Figure 4F,G). MDA-MB 468 cells treated with or without MY05 were fixed and permeabilized, after which they were incubated with MYC and MAX antibodies raised in different species.

https://doi.org/10.1021/acs.jmedchem.4c02556
J. Med. Chem. 2025, 68, 6233−6251

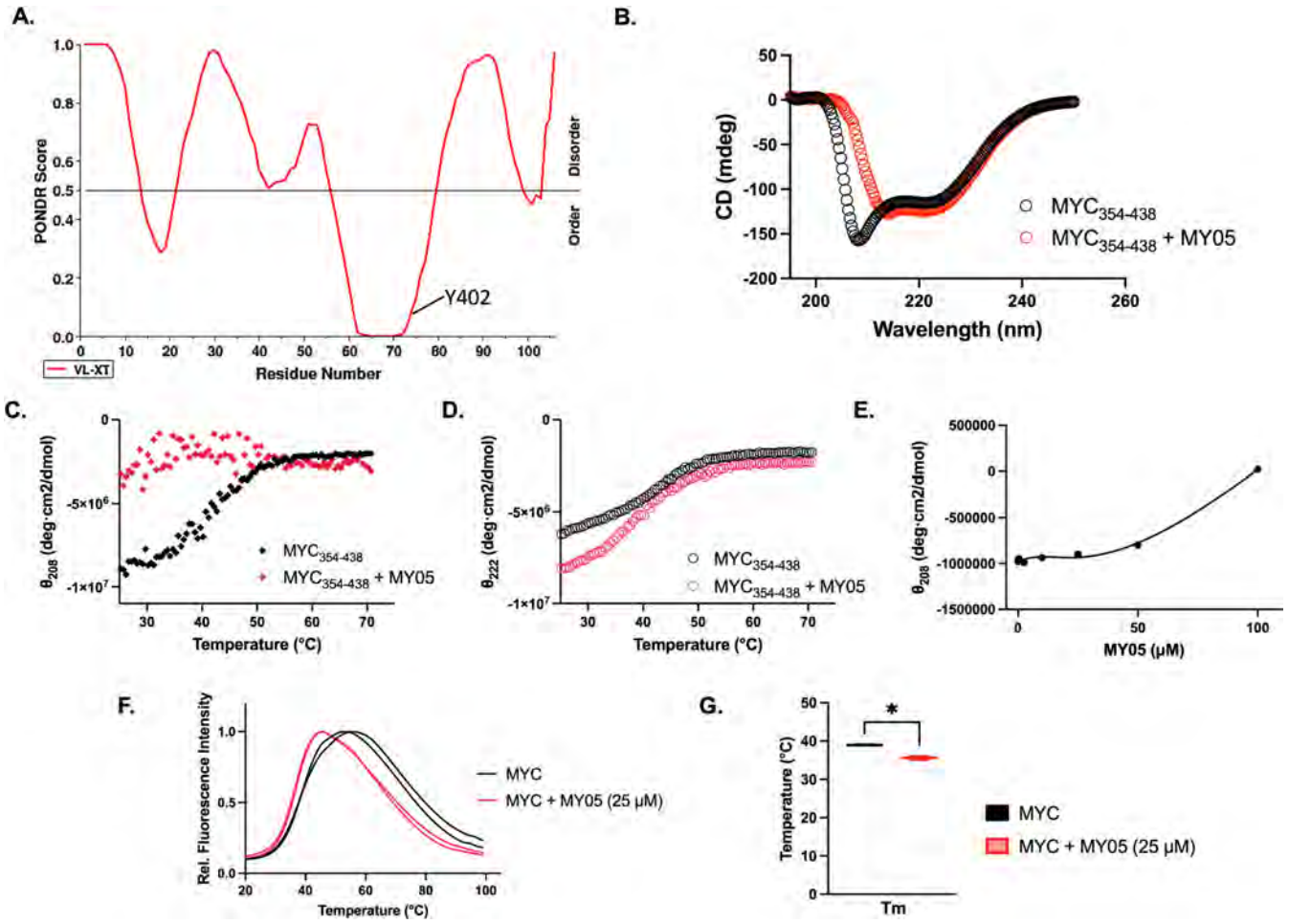

Figure 3. Solution phase conformations. (A) PONDR[67] score analysis of the degree of order and disorder in $MYC_{354-438}$. CD showing changes in the ellipticity of MYC (black) and the MY05−MYC (red) protein complex at (B) room temperature, (C) variable temperature monitored at 208 nm, and (D) variable temperature monitored at 222 nm. (E) Plot of the ellipticity of MYC titrated against varying concentrations of MY05 monitored at 208 nm. (F) Boltzmann plot of the polymerase chain reaction (PCR)-based protein thermal shift assay of MYC and MY05−MYC and (G) plot of the respective derived melting temperatures. The raw data are fit with equations for the unfolding of the monomers. Data represented as mean ± SD, $n = 2$, and analyzed by unpaired Student's t-test ($^*p < 0.05$).

Secondary antibodies of corresponding primary antibody origin, which are conjugated with fluorescently labeled oligonucleotide probes, were then added to interact with primary antibodies. These probes individually attached to MYC or MAX will only hybridize when in proximity and ligate to form circular DNA. Hybridization and ligation of fluorescent DNA probes are expected in MYC−MAX dimers but not the MYC monomer. An amplification step follows the ligation, where the circular DNA is amplified to intensify fluorescence, which can then be visualized by fluorescence microscopy as PLA dots for each dimer. The reduced number of PLA dots observed in treated compared to control groups indicates the reduced MYC−MAX dimer present, which we posit is due to the disruption of MYC−MAX heterodimerization by MY05.

Active MYC is found in the heterodimerized form with MAX. To examine the effect of MY05 on active MYC, an MYC transcription factor activity assay was used. The assay employs a dsDNA-coated plate with a canonical c-MYC binding sequence and uses colorimetric detection to analyze c-MYC in nuclear extracts or lysates. Here, nuclear extracts from P493-6- or MDA-MB-468-treated or untreated cells were freshly isolated and incubated in coated plates. Subsequent MYC antibody capture and HRP-conjugated secondary antibody detection revealed that MY05 and its close analogue MY04 induce reduced levels of active MYC, providing additional evidence for MYC−MAX disruption (Figure 4H,I).

MY05 Reduces MYC Protein Levels. A significant reduction in MYC protein levels was observed in MDA-MB 468 cells and P493-6 cells following a 24 h treatment of MY05 in a dose-dependent manner (Figure 5A). Next, intracellular MYC protein stability was evaluated by using the cycloheximide chase assay. We found that MY05 reduced the MYC protein half-life from 60 to 20 min in P493-6 cells (Figure 5B). Thus, we hypothesized that the decrease in MYC levels is driven by proteasomal degradation. To test this, cells were pretreated with the proteasome inhibitor MG132 to examine the rescue of MYC depletion following MY05 treatment. There was pronounced MYC protein stabilization with the increasing concentration of MY05 up to 50 μM in the presence of MG132 in MDA-MB-468 cells (Figure 5C). In a time-dependent manner, we monitored MYC and FBXW7 levels in MDA-MB-468 cells treated with MY05 at 25 μM and observed a reduction in MYC levels starting at 9 h of treatment and up to 24 h (Figure 5D). Since the MYC phosphorylation cascade is known to regulate the protein's stability, we examined the

https://doi.org/10.1021/acs.jmedchem.4c02556
J. Med. Chem. 2025, 68, 6233−6251

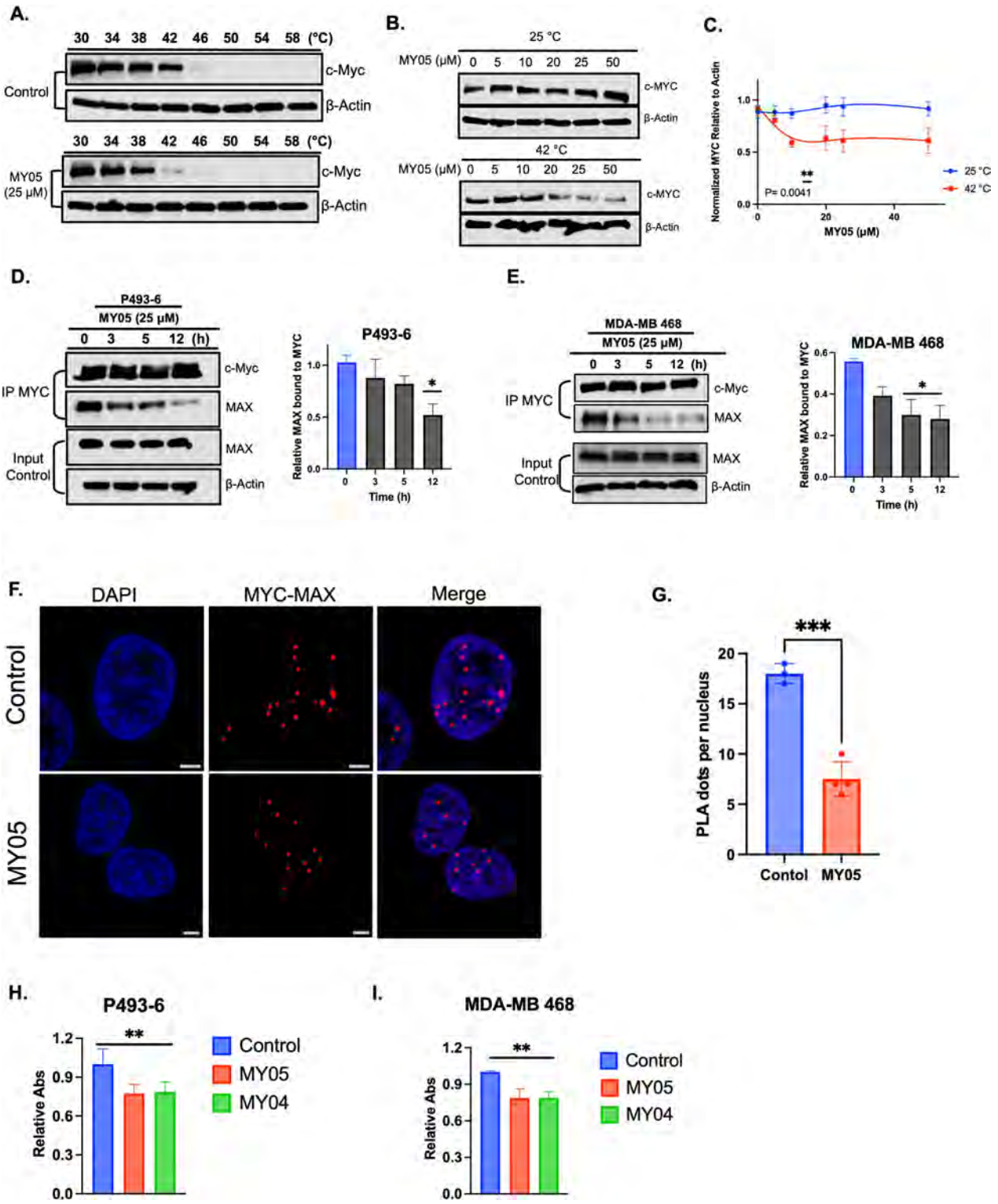

Figure 4. Intracellular MYC target engagement of MY05. Western blots showing MYC protein levels in CETSA in P493-6 cells treated with MY05 or DMSO control (A) at varying temperatures between 30 and 58 °C and (B) at varying concentrations of MY05 under isothermal conditions and (C) melt curve of MYC protein levels at varying concentrations of MY05 under isothermal conditions. Co-immunoprecipitation of MYC and MAX showing MAX levels after 0, 3, 5, and 12 h treatment of MY05 in (D) P493-6 and (E) MDA-MB 468, and the respective quantification of the relative MAX bound to MYC. (F) Immunofluorescence image of MYC−MAX in a proximity ligation assay in MDA-MB 468 cells treated or untreated with 25 μM MY05 for 12 h. Each red dot represents the MYC−MAX protein within proximity, indicative of heterodimerization; scale bar:4 μm. (G) Graph showing the number of PLA dots. Data analyzed by unpaired Student's *t*-test (***$p < 0.001$). (H) Transcription factor activity assay represented as a graph showing levels of active MYC treated with 25 μM MY05 and MY04 or untreated (control) in P493-6 cells and (I) MDA-MB 468. The error bar represents mean ± SD, $n = 6$. Data were analyzed by one-way analysis of variance (ANOVA), followed by Dunnett's multiple test (**$p < 0.01$, * $p < 0.05$).

https://doi.org/10.1021/acs.jmedchem.4c02556
J. Med. Chem. 2025, 68, 6233−6251

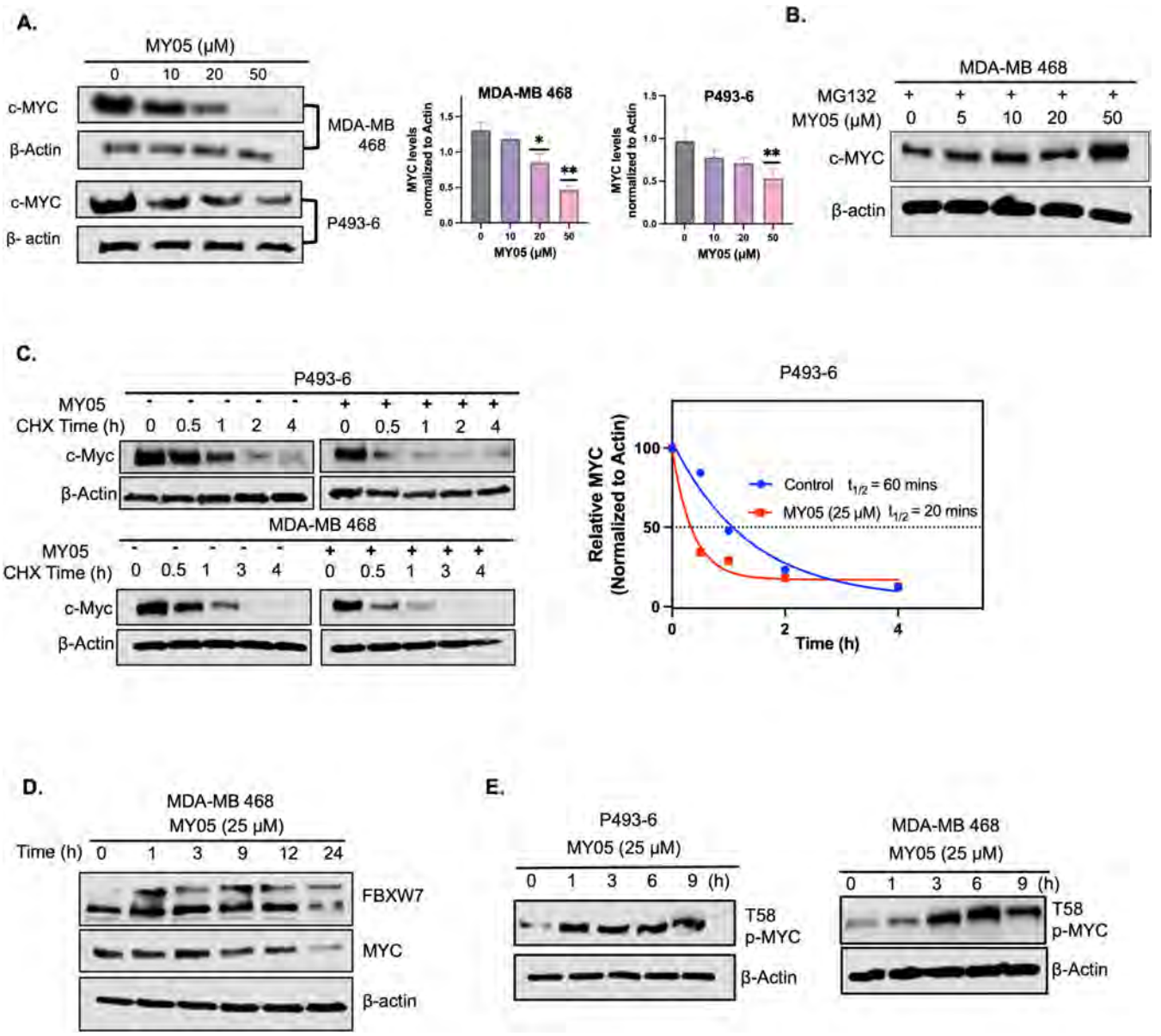

Figure 5. Downstream effectors of MYC inhibition by MY05. (A) Western blot showing MYC levels in MDA-MB 468 and P493-6 cells upon treatment with MY05 at the shown concentration for 24 h and the respective quantification of the MYC levels normalized to actin. The error bar represents mean ± SD, $n = 2$. Data were analyzed by one-way ANOVA, followed by Dunnett's multiple test (**$p < 0.01$, *$p < 0.05$). (B) MYC levels in MDA-MB 468 cells pretreated with proteasome inhibitor MG132, followed by treatment with the shown concentrations of MY05 or DMSO for 24 h. (C) Western blots showing MYC levels with or without MY05 treatment in P493-6 and MDA-MB 468 cells upon treatment with CHX and the half-life plot of the cycloheximide chase assay in P-4936 cells. (D) Western blot showing MYC and FBXW7 levels in MDA-MB 468 cells upon treatment with MY05 over the indicated time. (E) Western blot showing levels of phosphorylated MYC at T58 upon treatment with MY05 (25 μM) at shown times in MDA-MB 468 and P493-6.

time-dependent effect of MY05 treatment on MYC in cells via western blot. Activation of phosphorylated threonine 58 (T58) on MYC was prominent by 3−9 h in MDA-MB-468 cells and by 1 h in P493-6 cells (Figure 5E). It is possible that the T58 phosphorylation events prime MYC for subsequent depletion in the phosphorylation cascade, consistent with literature reports on MYC stabilization and destabilization.[75−78]

MY05 Attenuates MYC-Regulated Transcriptional Activities. Next, we sought to understand the effect of MY05 on global gene expression and MYC target genes using bulk RNA sequencing. Three independent samples of MDA-MB 468 cells were either exposed to 25 μM MY05 for 24 h or untreated; the total RNA expressed was extracted and sequenced at 30 million reads per sample, paired-end 50 base pairs. A total of 968 genes were found to be significantly differentially expressed (Figure 6A). Gene Ontology (GO) enrichment analysis with the topmost significant terms showed that genes involved in cellular division and cell cycle regulation were downregulated, potentially stifling cell growth processes, while genes in response to cellular stress were upregulated (Figure 6C,D). We found that MY05 treatment reduced the mRNA levels of well-established MYC target genes including kinases that regulate cell maturation, growth, and division, as shown in Figure 6E. Further confirmation using qRT-PCR showed the reduction in the expression levels of CCNA2, CDK2, CDK1, CDC25A, CDC25C, E2F1, E2F2, and SKP2 in

https://doi.org/10.1021/acs.jmedchem.4c02556
J. Med. Chem. 2025, 68, 6233−6251

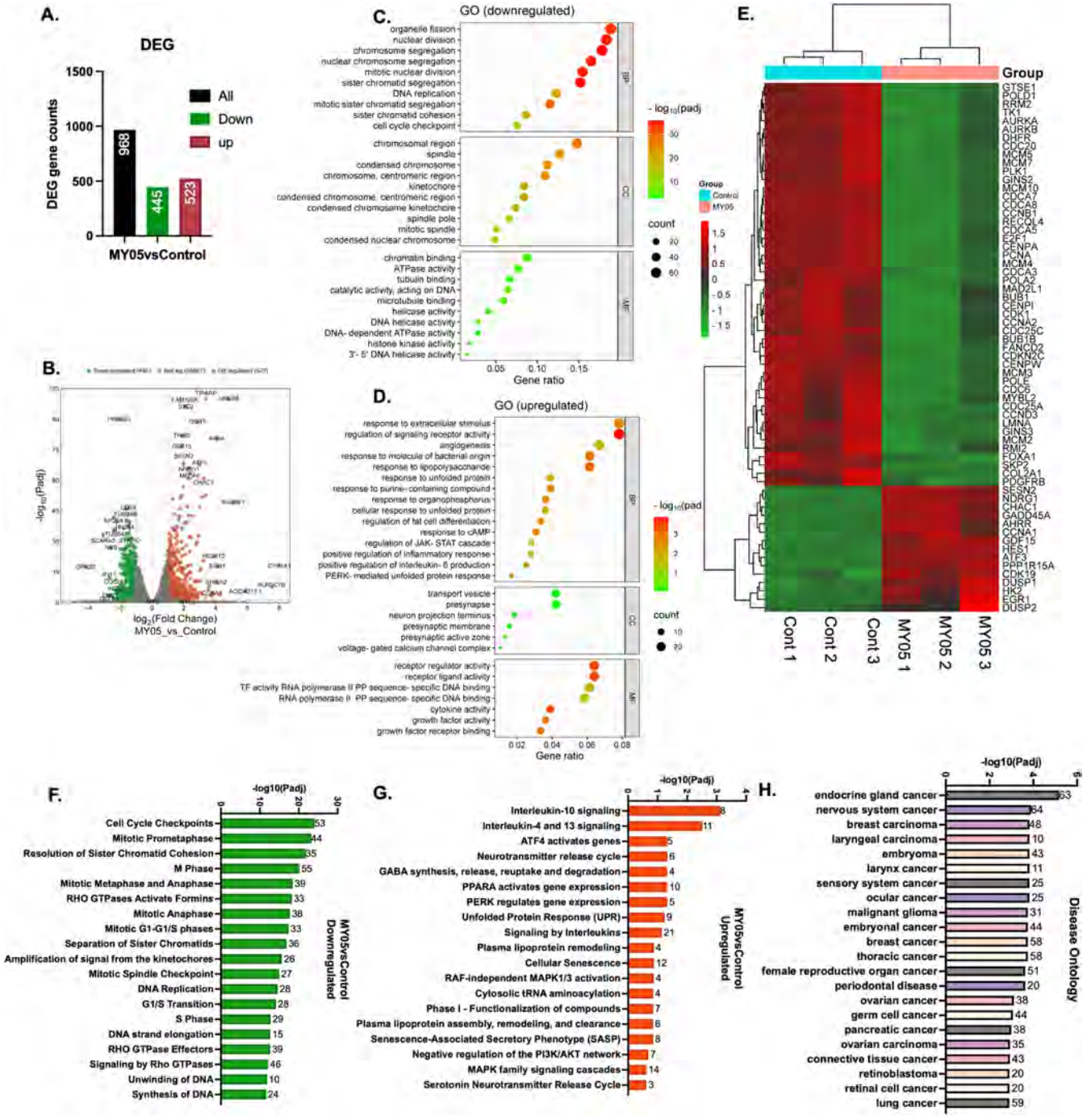

Figure 6. MY05 induces changes in the gene expression profile. (A) Bar graph showing the number of significant differentially expressed genes determined by bulk RNA sequencing. (B) Volcano plot of gene expression levels in MDA-MB 468 upon treatment with MY05 compared to untreated cells. (C) Gene ontology of differentially expressed genes that are downregulated and (D) upregulated upon treatment with MY05, with genes grouped based on the biological process (BP), cellular component (CC), or molecular function (MF). (E) Heat map showing expression levels of select target genes of MYC in cells treated with or without MY05. (F) Reactome pathway analysis of top significantly enriched genes that are downregulated or (G) upregulated upon treatment with MY05. (H) Disease ontology of differentially expressed genes with MY05 treatment.

MDA-MB 468 or P493-6 cells from as early as 12 h of treatment (Figure S54C,D) with most significant reduction observed with 48 h of treatment (Figure S54E). Pathway analysis using the Reactome database showed that the top downregulated genes were majorly involved in cellular division processes, which MYC is known to strongly regulate as a transcription factor (Figure 6F), whereas in response to the treatment of MDA-MB 468 cells with MY05, genes involved in inflammatory and stress responses leading to cell death were expressed (Figure 6G). Analysis of the disease ontology shows that the studied genes, like MYC protein, are implicated in similar types of cancers (Figure 6H). Taken together, MY05 engages and reduces MYC levels to frustrate the MYC transcriptional program.

MY05 Promotes Apoptosis and Inhibits MYC-Driven Mammosphere Growth. To examine the mode of cell death

https://doi.org/10.1021/acs.jmedchem.4c02556
J. Med. Chem. 2025, 68, 6233−6251

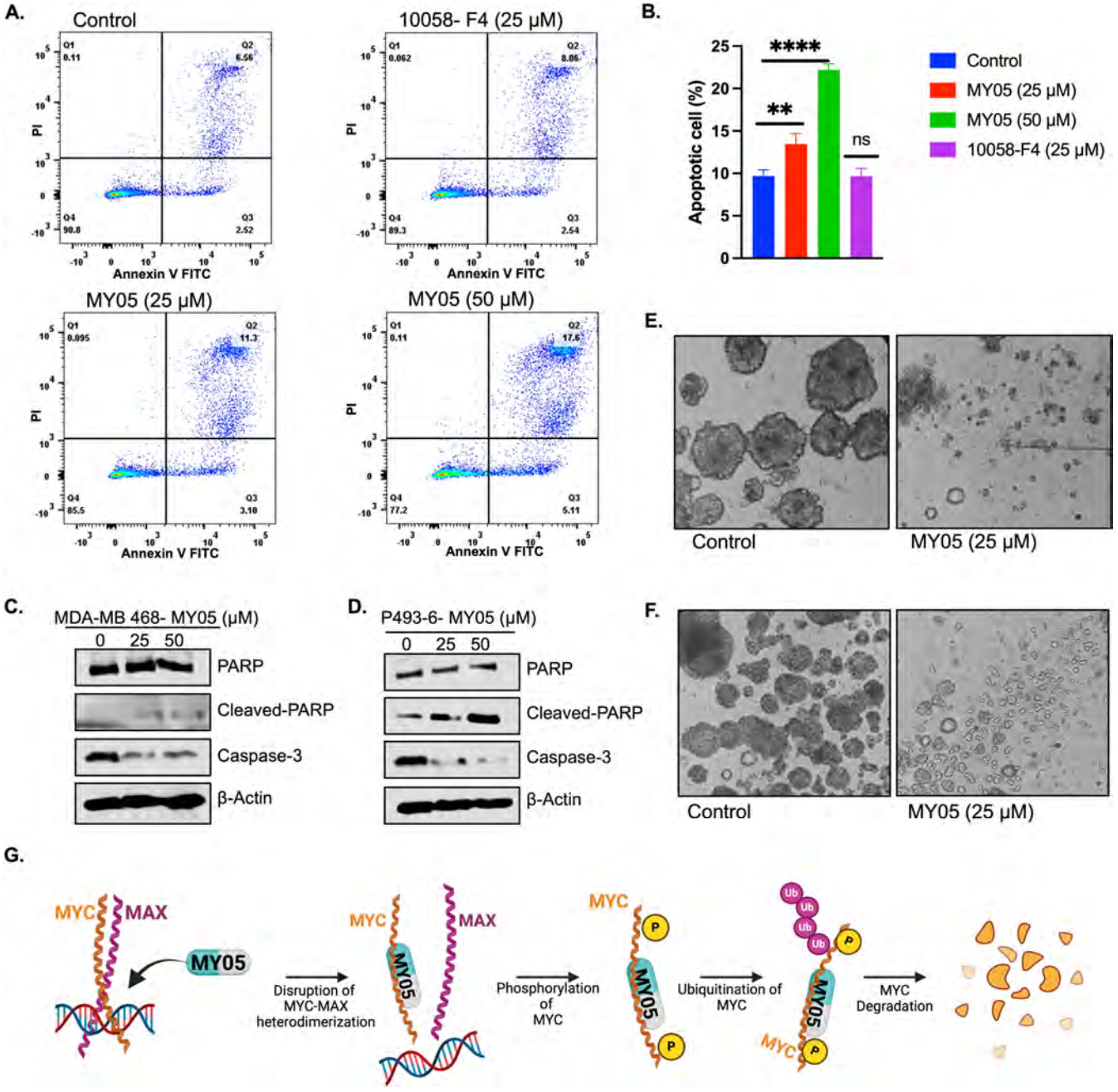

Figure 7. MY05 potentiates MYC-driven cellular responses. (A, B) Apoptotic plot showing live cells (Q4), early apoptotic (Q3), and late populations (Q2) and necrotic cells (Q1) in (A) and a bar chart of the total apoptotic population of treated cells compared to the control in (B) in P493-6 cells treated with 10058-F4 (25 μM) as a positive control, MY05 at 25 and 50 μM or DMSO for 24 h. The error bar represents mean ± SD, $n = 3$. Data were analyzed by one-way ANOVA, followed by Dunnett's multiple test (****$p < 0.0001$, **$p < 0.01$). (C, D) Western blot showing levels of apoptosis markers in MDA-MB 468 (C) and P493-6 cells (D) treated with MY05 at 25 and 50 μM or DMSO for 24 h. (E, F) Mammosphere formation of MCF-7 (E) and MDA-MB 468 cells (F) after 5 days of treatment of 25 μM MY05 or control. (G) Plausible mechanism of engagement and regulation of MYC by MY05. Image generated by BioRender.

imposed by MY05, the dual staining fluorescence-activated cell sorting (FACS) analysis using Annexin V and PI was used. 10058-F4 and MY05-treated or untreated cells for 24 h were stained and analyzed appropriately (Figure 7A,B). A dose−response increase in early- and late-stage apoptosis was found in cells treated with MY05 compared to 10058-F4. Markers of apoptosis such as caspase-3, PARP, and cleaved-PARP[79] in both MDA-MB-468 and P493-6 cells confirmed the induction of apoptosis by MY05 (Figure 7C,D). 3D spheroids recapitulate the human tumor.[80] The ability of MY05 to inhibit 3D mammosphere growth was studied by forming mammosphere in ultralow adherent plates and exposing them to MY05. After 5 days of incubation, no visible mammosphere was noticeable in the treated wells compared to the control (Figure 7E,F). The sensitivity of the MYC-driven mammosphere to MY05 demonstrates the translational potential of this novel scaffold to inhibit MYC activities in cancer. We propose that MYC's activity is regulated by MY05 via intracellular engagement, which triggers disruption of the MYC−MAX dimer, priming the MYC monomer for phosphorylation and

https://doi.org/10.1021/acs.jmedchem.4c02556
J. Med. Chem. 2025, 68, 6233−6251

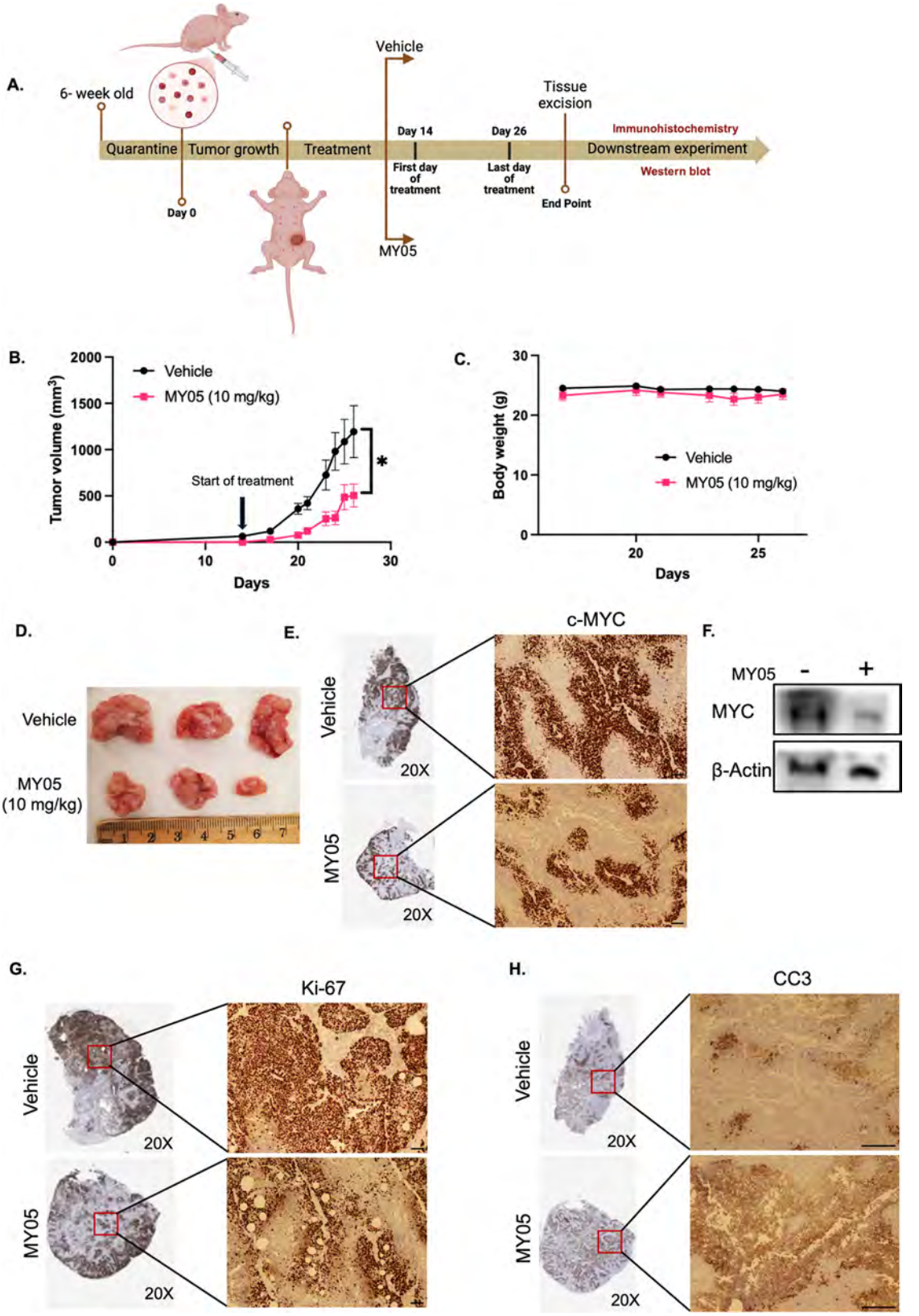

Figure 8. MY05 inhibits tumor progression in mice. (A) Workflow chart of *in vivo* studies. (B) Plot showing the inhibitory effect of MY05 on tumor volume and (C) body weight of MDA-MB 468-inoculated Nu/J mice. Error bars represent mean ± standard error mean (SEM), $n = 4$. Data were analyzed by the unpaired *t*-test (*$p < 0.05$) (D) Images of the excised tumor from mice treated with vehicle or MY05 at the endpoint. (E) Quantification of MYC levels in the tumor at the endpoint by immunostaining and (F) western blot in mice treated with vehicle or MY05. (G) IHC staining of tumor slices quantifying K_i-67 and (H) cleaved caspase-3 (CC3) levels at the endpoint.

https://doi.org/10.1021/acs.jmedchem.4c02556
J. Med. Chem. 2025, 68, 6233−6251

subsequent degradation via ubiquitination (Figure 7G). We then sought to further investigate the inhibitory potential of MY05 in a more complex *in vivo* system.

MY05 Inhibits MYC-Driven Solid Tumor Growth. Therapeutic indices of MY05 were assessed using the MDA-MB 468 TNBC mouse model. MDA-MB 468 is MYC-driven and was used in our proof-of-concept studies throughout this report serving a strong rationale for the use of this model to validate *in vivo* effects. The efficacy of MY05 was initiated with MDA-MB-468 orthotopic tumor inoculation and randomization after tumors reached >50 mm^3. Mice were treated with MY05 or the vehicle control (33% DMSO, 67% Kolliphor) every other day subcutaneously. We found that MY05 induced significant tumor growth inhibition compared to control as measured by calipers using the elliptical measurement method (Figure 8A,C). MY05 was well tolerated in mice, as no changes in body weight were observed in the duration of the study (Figure 8B). Further, pharmacodynamic assessments using immunohistochemistry (IHC) coupled with orthogonal western blots demonstrated reduced expression of MYC in MY05-treated mice tissue compared to the control, indicative of the significant target engagement of MYC by MY05 (Figure 8D,E). IHC staining also revealed that MY05 suppressed proliferation and induced apoptosis in tumor tissue, as evidenced by the downregulation of ki-67, a proliferation marker, and upregulation of cleaved caspase-3, which is a bonafide marker of apoptosis (Figure 8F). In summary, these results highlight MY05 as a potential therapeutic for MYC-driven cancers.

DISCUSSION AND CONCLUSIONS

Targeting MYC for regulation has long been the goal of many drug discovery efforts for cancer treatment due to the established inductive effect of unchecked MYC levels in the progression of many cancers.[81] Of the many strategies employed for the inhibition of MYC transcriptional activity is the disruption of MYC's dimerization with its obligate partner MAX, preventing interactions with the DNA, thereby stunting the MYC transcriptional program.[9,82−85]

In this study, through guided *in silico* modeling directing the selection of chemotypes interacting with hotspots of MYC similar to those of 10058-F4, we discovered a novel dihydro pyrazolo pyridinone chemotype. Through this robust process, we discovered that the identified chemotype interacted with the Tyr402 of MYC, which was further developed into MY01. MY01 significantly inhibited active MYC levels driving transcription in P493-6 cells. The initial compound was then expanded into a library of seven compounds, of which MY05 was identified as the lead candidate with an attractive balance of potency and MYC selectivity.

Ligand interaction with a protein could induce structural changes, which may in turn inform changes in the functional dynamics of the protein.[86,87] By expressing a truncated version of MYC containing the proposed MY05 binding region as indicated by initial *in silico* studies, we determined that MY05 interacted with MYC in solution and as a result induced changes in MYC's secondary structure. The observed structural change translated to a functional thermal instability of MYC upon interaction with MY05, with a reduction in the melting temperature of MYC-MY05 compared to that of apo MYC.

Protein−ligand interaction in solution may not exactly replicate cellular conditions with a myriad of interacting partners competing with a ligand for a binding spot with the protein of interest. By performing CETSA analysis, we were able to affirm that MY05 induced similar thermal behavior of MYC intracellularly as observed in solution, pointing toward selective intracellular MYC engagement by MY05. To this effect, we observed inhibition of MYC's transcriptional activities, which we attributed to the induced disruption of the MYC−MAX heterodimerization by MY05.

By inhibiting MYC−MAX heterodimerization and inducing MYC thermal instability, we were able to decrease its half-life through proteasomal degradation, hence reducing available endogenous MYC for transcription activation. MYC's role in cancer progression is delivered through the activities of target genes.[88] Active MYC transcription is a consequence of MYC−MAX interaction; therefore, the disruption of the heterodimer compromises the transcriptional program of MYC and its attendant gene expression profile in cells. Global gene expression profiling within cells revealed that several target genes implicated in cell growth, proliferation, division, differentiation, and metabolism were modulated by MY05-induced disruption of MYC−MAX, suggestive of altered expression of MYC-regulated genes. The combination of all of these resulted in the inhibition of MYC-associated cellular responses. MY05 treatment induced cell death by apoptosis and inhibited the formation of mammosphere *in vitro* and tumor growth *in vivo*, serving as an indication of the tumor progression inhibitory properties of the compound. This compound is one of the few MYC-targeting small molecules that inhibit solid tumor growth in a cancer mouse model. Our observation is critical to advancing the field of therapeutic small-molecule MYC-targeting agents. Several small molecules have been unsuccessful due to the lack of rigorous *in vivo* preclinical characterization, and MY05 discovery and development have changed that narrative. We believe that the promising *in vivo* data obtained for MY05 and the preclinical/first-in-human trials of Omomyc provide impetus to drive further development of MY05.[89,90]

The overexpression of MYC in highly proliferating cells, coupled with its role in cell division and development, marks it as a worthy target for the treatment of cancer. Expanding the library of available MYC inhibitors would greatly advance the discovery of selective and potent small molecules targeting MYC for cancer treatment. In summary, our contribution through this work has helped to advance the discovery of a selective MYC inhibitor.

EXPERIMENTAL SECTION

General Information. Reagents and solvents used for synthesis were purchased from commercial vendors (Acros, Millipore-Sigma, USA) and used without further purification unless otherwise stated. Acetonitrile (CH_3CN) and dimethylformamide (DMF) were used from an Acros Seal anhydrous bottle containing 3 Å molecular sieves. Dry dichloromethane (CH_2Cl_2) was distilled over CaH_2 and stored over 4 Å molecular sieves in an anhydrous solvent bottle. Tetrahydrofuran (THF) was distilled from a mixture of sodium metal and benzophenone ketyl under nitrogen. Synthesized compounds were purified by silica gel flash chromatography, and the purity of compounds was assessed to be >97% by reversed phase high-performance liquid chromatography (RP-HPLC). The HPLC data were obtained on an Agilent 1100 series HPLC using a normal phase column.

Nuclear magnetic resonance spectroscopy (^1H, ^{13}C NMR) was recorded on a Varian Unity 400/500 NMR instrument with a Spectro Spin superconducting magnet in the University of Kentucky NMR Facility. The coupling constant, *J*, was reported in the Hertz unit (Hz). Chemical shifts were reported in ppm; ^1H NMR spectra were

https://doi.org/10.1021/acs.jmedchem.4c02556
J. Med. Chem. 2025, 68, 6233−6251

internally referenced to solvent signals (^{1}H NMR: DMSO at δ = 2.50 ppm, CD_3CN at δ = 1.94 ppm, ^{13}C NMR: DMSO δ = 39.52 ppm). Column chromatography was done on a Combi-Flash from Teledyne ISCO. Mass spectra were obtained on an Advion low-resolution mass spectrometer using the electrospray ionization (ESI) method.

A. Standard Method for the Synthesis and Physical Characterization and Discovery of MYC Inhibitors. 1. Standard Method for the Synthesis of ***1****.* To a solution of KCN (2 equiv) in distilled water (100 mL) was added MeOH (100 mL) at room temperature. To the rapidly stirring solution was added a solution of 2-bromo-arylketone (1 equiv) in EtOH (200 mL). After 20 min, ice (100 mL) and 1 M HCl (30 mL) were added. The resultant precipitate was filtered and washed with copious amounts of water. The wet solid was transferred to a beaker and titrated with 5% ethyl acetate in hexanes (100 mL). The solid was filtered and washed with hexanes to yield the target aryloxopropanenitrile compounds.

*2. Standard Method for the Synthesis of Pyrazol-5-Amine Compounds (****2****).* To a solution of aryloxopropanenitrile (1 equiv) in ethanol (10 mL) was added (2-methylphenyl)hydrazine hydrochloride (2.15 g, 13.5 mmol). The reaction was stirred at 80 °C for 16 h and then cooled to rt. It was concentrated under reduced pressure, and the residue was purified by silica gel flash chromatography (20−30% = hexanes/ethyl acetate) to afford the target pyrazol-5-amine compounds.

*3. Standard Method for the Synthesis of 4-Formyl-pyrazolyl-dimethylimidoformamides (****3****).* A solution of pyrazol-5-amine derivatives (1.0 equiv) and $POCl_3$ (1.2 equiv) in DMF solution (3 mL) was stirred at 75 °C for 5 h. When the reaction was completed, as confirmed via thin-layer chromatography (TLC), the reaction mixture was concentrated, added to water (10 mL), and extracted with CH_2Cl_2 (20 mL). The organic extracts were washed with saturated $NaHCO_3$, dried over $MgSO_4$, filtered, and concentrated under reduced pressure. The residue solution was purified by column chromatography on silica gel (30−50% = hexanes/ethyl acetate) to give the corresponding target compounds.

*4. Standard Method for the Synthesis of 5-Amino-4-formylpyrazole Compounds (****4****).* A solution of 4-formyl-pyrazolyl-dimethylimidoformamide derivatives (1.0 equiv) and NaOH (2.0 equiv) in MeOH solution (15 mL) was refluxed for 3 h. When the reaction was completed, the reaction mixture was concentrated to remove the solvent, added to water (10 mL), and extracted with CH_2Cl_2 (20 mL). The organic extracts were washed with saturated $NaHCO_3$, dried over $MgSO_4$, filtered, and concentrated under reduced pressure. The residue solution was purified by short-column chromatography on silica gel to give the corresponding 5-amino-4-formylpyrazole target compounds.

*5. Standard Method for the Synthesis of Pyrazolo[3,4-b]pyridin-6-one Derivatives (****5****).* A solution of 5-amino-4-formylpyrazole derivatives (1.0 equiv), piperidine (3 equiv), and ethylcyanoacetate (1.2 equiv) in ethanol solution (15 mL) was stirred at 90 °C for 5 h. When the reaction was completed, as confirmed via TLC, the reaction mixture was cooled, concentrated, added to water (10 mL), and extracted with CH_2Cl_2 (20 mL). The organic extracts were washed with saturated $NaHCO_3$, dried over $MgSO_4$, filtered, and concentrated under reduced pressure. The residue solution was purified by column chromatography on silica gel (30−50% = hexanes/ethyl acetate) to give the corresponding pyrazolo[3,4-*b*]pyridin-6-one target compounds.

MY01. ^{1}H NMR (400 MHz, DMSO-d_6) δ 9.11 (d, J = 8.2 Hz, 4H), 7.86 (s, 2H), 7.45 (s, 2H), 7.29 (s, 2H), 7.19 (s, 1H), 2.37 (s, 3H). ^{13}C NMR (101 MHz, DMSO-d_6) δ: 164.78, 138.66, 134.28, 130.49, 129.93, 129.12, 128.72, 127.20, 103.81, 22.89. Purity was determined to be 99% by RP-HPLC: flow rate: 1 mL/min; λ = 280 nm; eluent A = DI water with 0.1% trifluoroacetic acid; eluent B = methanol with 0.05% formic acid; solvent gradient: 0−3 min (100:0 H_2O/MeOH), 3−5 min (50:50 H_2O/MeOH), 5−7 min (40:60 H_2O/MeOH), 7−8 min (30:70 H_2O/MeOH), 8−10 min (0:100 H_2O/MeOH), 10−12 min (20:80 H_2O/MeOH), 12 min−end of run (100:0 H_2O/MeOH).

MY02. ^{1}H NMR (400 MHz, DMSO-d_6) δ 13.22 (s, 1H), 8.97 (s, 1H), 8.21 (d, J = 7.8 Hz, 2H), 8.03 (d, J = 8.8 Hz, 2H), 7.60−7.52 (m, 2H), 7.36 (t, J = 7.4 Hz, 1H), 7.10 (d, J = 8.9 Hz, 2H), 3.85 (s, 3H). ^{13}C NMR (101 MHz, DMSO-d_6) δ: 170.29, 167.35, 159.03, 152.44, 129.57, 129.02, 127.67, 121.77, 121.08, 120.85, 114.94, 55.78. Purity was determined to be 99% by RP-HPLC: flow rate: 1 mL/min; λ = 280 nm; eluent A = DI water with 0.1% trifluoroacetic acid; eluent B = methanol with 0.05% formic acid; solvent gradient: 0−3 min (100:0 H_2O/MeOH), 3−5 min (50:50 H_2O/MeOH), 5−7 min (40:60 H_2O/MeOH), 7−8 min (30:70 H_2O/MeOH), 8−10 min (0:100 H_2O/MeOH), 10−12 min (20:80 H_2O/MeOH), 12 min−end of run (100:0 H_2O/MeOH).

MY03. ^{1}H NMR (400 MHz, DMSO-d_6) δ 8.39 (dd, J = 8.0, 4.0 Hz, 2H), 8.34 (s, 1H), 8.02 (dd, J = 8.0, 4.0 Hz, 2H), 7.31 (t, J = 8.0 Hz, 4H). ^{13}C NMR (101 MHz, DMSO-d_6) δ: 161.44, 156.02, 143.55, 137.37, 136.94, 129.67, 129.28, 121.95, 121.44, 116.31, 116.09, 115.86, 115.63, 102.60, 97.30. ^{19}F NMR (376 MHz, DMSO-d_6) δ: −113.24, −118.59. Purity was determined to be >97% by RP-HPLC: flow rate: 0.5 mL/min; λ = 260 nm; eluent A = DI water with 0.1% trifluoroacetic acid; eluent B = acetonitrile with 0.05% formic acid; solvent gradient: 0−4 min (100:0 H_2O/ACN), 4−10 min (0:100 H_2O/ACN), 10−17 min (100:0 H_2O/ACN), 17 min−end of run (50:50 H_2O/ACN),

MY04. ^{1}H NMR (400 MHz, DMSO-d_6) δ: 9.14 (s, 1H), 8.16 (dd, J = 14.5, 8.2 Hz, 4H), 7.60 (t, J = 8.7 Hz, 4H), 7.42 (t, J = 7.4 Hz, 1H). ^{13}C NMR (101 MHz, DMSO-d_6) δ: 144.22, 138.62, 134.47, 130.57, 129.70, 129.36, 127.41, 122.28. Purity was determined to be >97% by RP-HPLC: flow rate: 0.5 mL/min; λ = 280 nm; eluent A = DI water with 0.1% trifluoroacetic acid; eluent B = acetonitrile with 0.05% formic acid; solvent gradient: 0−4 min (100:0 H_2O/ACN), 4−10 min (0:100 H_2O/ACN), 10−17 min (100:0 H_2O/ACN), 17 min−end of run (50:50 H_2O/ACN),

MY05. ^{1}H NMR (400 MHz, DMSO-d_6) δ: 9.12 (s, 1H), 8.16 (dd, J = 14.5, 8.2 Hz, 4H), 7.60 (t, J = 8.7 Hz, 4H), 7.42 (t, J = 7.4 Hz, 1H). ^{13}C NMR (101 MHz, DMSO-d_6) δ: 144.22, 138.62, 134.47, 130.57, 129.70, 129.36, 127.41, 121.84. Purity was determined to be >97% by RP-HPLC: flow rate: 1 mL/min; λ = 280 nm; eluent A = DI water with 0.1% trifluoroacetic acid; eluent B = methanol with 0.05% formic acid; solvent gradient: 0−3 min (100:0 H_2O/MeOH), 3−5 min (50:50 H_2O/MeOH), 5−7 min (40:60 H_2O/MeOH), 7−8 min (30:70 H_2O/MeOH), 8−10 min (0:100 H_2O/MeOH), 10−12 min (20:80 H_2O/MeOH), end of run (100:0 H_2O/MeOH).

MY06. ^{1}H NMR (400 MHz, DMSO-d_6) δ 9.07 (s, 1H), 7.97 (d, J = 8.1 Hz, 4H), 7.35 (d, J = 8.0 Hz, 2H), 7.13 (d, J = 9.1 Hz, 2H), 3.84 (s, 3H), 2.39 (s, 3H). ^{13}C NMR (101 MHz, DMSO-d_6) δ 161.45, 139.26, 130.11, 127.46, 116.79, 114.80, 55.98, 46.85, 43.00.

MY07. ^{1}H NMR (400 MHz, DMSO-d^6) δ: 9.10 (s, 1H), 8.28 (d, J = 8.9 Hz, 2H), 8.00 (d, J = 8.1 Hz, 2H), 7.66 (d, J = 9.0 Hz, 2H), 7.35 (d, J = 7.9 Hz, 2H), 2.40 (s, 3H). ^{13}C NMR (101 MHz, DMSO-d_6) δ: 161.45, 130.15, 129.63, 127.59, 116.79, 46.85, 43.00, 21.41.

6. In Silico Studies. A library of compounds (100,000) was prepared by carefully selecting compounds from the ZINC and MOE library (xLog $P \leq 2.5$; MW ≤ 500; the number of rotatable bonds of $\leq$5). The protein (PDB: 1NKP) was prepared using the MOE structure preparation wizard. Hydrogen atoms were added, and the protonation states were assigned using the Protonate-3D tool at pH 7.4. The possible active sites were determined, and the MYC402−412 site was specified using the Site Finder application in MOE and then earmarked with dummy atoms. Then, a library of 100,000 diverse small molecules was docked against the modeled MYC protein. This was followed by two-stage molecular docking calculations: an initial induced-fit docking based on London dG scoring and a secondary refinement based on the GBVI/WSA dG scoring function. The top-scoring 1% molecules were selected and validated via redocking into the protein. Then, PAINS filters were applied to the selected top 1% hits, and subsequent physical analysis of their interacting amino in their binding pockets, as well as a careful analysis of their predicted ADMET properties, was performed.

B. Standard Method for In Vitro Biological Studies. 7. Recombinant Protein Expression and Purification. Plasmid (pET28a backbone) encoding 6x His-tag human MYC bHLHZip domain ($MYC_{354-438}$) and MAX (80 amino acids) was received from

https://doi.org/10.1021/acs.jmedchem.4c02556
J. Med. Chem. 2025, 68, 6233−6251

Giovanni Zinzalla at Karolinska Institutet (Stockholm, Sweden). *Escherichia coli* (BL21(DE3)) competent bacteria cells (New England Biolabs) were transformed with the plasmid following the product manual transformation protocol. A single colony of transformed bacteria was inoculated in 10 mL of Luria−Bertani (LB) medium containing 50 μg/mL kanamycin and grown overnight at 37 °C, 250 rpm in an orbital shaker. Overnight culture was then transferred into 1 L of LB medium (1:100 overnight: main culture), and the cells were further grown for 5 h to an OD_{600} of about 0.8, followed by an induction of protein expression by adding 0.4 mM isopropyl-L-thio-β-D-galactopyranoside (IPTG, Thermo Fisher Scientific). The cells were grown for additional 8 h after which they were harvested by centrifugation at 10,000 rpm for 30 min at 4 °C. Cell pellet was lysed in denaturing conditions (100 mM $NaHPO_4$, 10 mM Tris-Cl, 8 M urea, 10 mM imidazole pH 8.0) by sonication. Lysate was centrifuged at 10,000 rpm for 30 min at 4 °C to pellet cell debris. Cleared lysate containing soluble proteins was then incubated with Ni-NTA resin (Thermo Fisher Scientific, HisPur) for 1 h. The resin-incubated cleared lysate was then loaded into a column and purified with an imidazole-gradient elution in non-denaturing conditions. Eluted protein was subjected to second size exclusion chromatography purification using Sephadex G-75 superfine resin (Cytiva). Pure protein fractions were collected and confirmed by sodium dodecyl sulfate-polyacrylamide gel electrophoresis (SDS-PAGE). MYC protein was then dialyzed into 50 mM phosphate buffer, pH 7.4, using a desalting column (Econo-Pac 10DG, Bio-Rad). Protein concentration was determined by the Bradford assay.

8. Circular Dichroism. MY05 stock concentration was prepared by dissolving in a minimal amount of DMSO. With PBS, MY05 was diluted to a working concentration of 1 mM. $MYC_{354-438}$ (15 μM) was prepared in the absence or presence of 25 μM MY05, 10058-F4, or 10054-G5. Circular dichroism spectra were recorded at 23 °C by using a Jasco-1100 spectrophotometer with a 1 mm path-length cuvette at 190−250 nm. Variable temperature experiments were monitored at 222 and 208 nm. For titration, individual samples of $MYC_{354-438}$ (15 μM) were prepared with indicated concentrations of MY05 (0.025−100 μM), and ellipticity was measured at 190−250 nm. Raw data collected were processed with Jasco software and plotted with GraphPad Prism.

9. Protein Thermal Shift Assay. The protein thermal shift assay was performed following the Applied Biosystems protocol. $MYC_{354-438}$ (2 μM) was prepared in PBS 1X pH 7.4 in a 96-well plate format in the absence or presence of 25 μM MY05. Protein thermal shift dye 8X (2.5 μL) (SYPRO orange, Applied Biosystems) was added to bring each well to a final assay volume of 20 μL. The plate was then sealed with optical adhesive film and centrifuged at 200 rpm for 2 min at 4 °C to collect the reaction mixture at the bottom and eliminate bubbles. The samples were analyzed with a ViiA 7 real-time PCR instrument (Applied Biosystems) with ramp rates of 1.6 and 0.05 °C/s for steps 1 and 2 at a 2 min temperature gradient for each step, respectively. The melt curves and melting temperature (T_m) were generated as processed by Protein Thermal Shift software, and graphs were plotted using GraphPad Prism.

10. Cell Culture. MDA-MB 231 and MDA-MB 468 cells were purchased from ATCC. MCF-7 was graciously supplied by Dr. Yadi Wu from the University of Kentucky. P493-6 cells were provided by Anne Le of Johns Hopkins University. MDA-MB 231, MDA-MB 468, and MCF-7 cell lines were cultured in Dulbecco's modified Eagle's medium (DMEM) with 10% fetal bovine serum (FBS), 1% penicillin/streptomycin, and 1% amphotericin B. P493-6 cells were cultured in a complete RPMI medium supplemented with 1% penicillin/streptomycin. All cells were grown in an incubator at 37 °C with 5% CO_2 in a humid atmosphere.

11. Cell Viability Assay. MDA-MB 468, MDA-MB 231, and MCF-7 cells were seeded at 2000 cells per 100 μL of media in 96-well plates. The cells were incubated overnight for them to adhere, after which they were treated with compounds at concentrations of 0.14−100 μM in a 150 μL total culture media volume. The cells were incubated for 96 h, and then the media were carefully aspirated off. The cells were rinsed with phosphate-buffered saline (PBS) and treated with 100 μL of 3-(4,5-dimethylthiazol-2-yl)-2,5-diphenyltetrazolium bromide (MTT) solution at 0.5 mg/mL concentration for 4 h in the dark. The spent MTT solution was removed from each well and replaced with 100 μL of DMSO. The absorbance was measured using a Biotek spectrophotometer plate reader at a wavelength of 570 nm.

P493-6 cells were seeded at 3000 cells per 100 μL of medium in sterile white-bottom 96-well plates. The cells were incubated overnight at 37 °C and then treated with test compounds to final concentrations between 0.14 and 100 μM. After 96 h of incubation, the cells were cooled to room temperature, and 50 μL of Cell Titer Glo solution (Promega) was added to each well. The cell plates were shaken in an orbital manner for 2 min and allowed to settle for 3 min. Luminescence measurement was taken using a Biotek plate reader at 1000 ms integration and 150 ms gain.

12. Modulation of MYC Expression. P493-6 cells were grown to 70% confluency, after which they were transferred into three T25 flasks containing complete RPMI growth media for high MYC expression, growth media supplemented with 0.1 μg/mL tetracycline and 1 μM β-estradiol for low MYC expression, or media containing only 0.1 μg/mL tetracycline to completely shut off MYC expression. The cells were grown for a further 72 h, and then the cell sizes were analyzed by fluorescence-activated cell sorting (FACS).

13. Western Blot. MDA-MB 468 and P493-6 cells in a fresh complete medium were plated (300,000 cells per well) into six-well plates for 24 h. This was followed by treatment with the DMSO control or compounds at the specified concentrations for 24 h. For MG132 treatment, the cells were pretreated with 30 μM MG132 for 1 h before compound treatment. The suspension cells were first harvested, pelleted by centrifugation, and washed with PBS. The cells were then lysed by the addition of Laemmli buffer. The Laemmli buffer was added directly to washed adherent cells in the well plates and scraped into Eppendorf tubes. Lysates were incubated at 90 °C on a heat block for 5 min. The cell samples were cooled and stored at −20 °C until ready for use. Whole-cell lysates were resolved by 4−20% sodium dodecyl sulfate-polyacrylamide gel electrophoresis (SDS-PAGE; 200 V for 35 min) followed by electro-transfer to a polyvinylidene difluoride membrane, PVDF (100 V for 1 h). The membranes were blocked in 3% (w/v) bovine serum albumin (BSA) in PBST for 1 h at room temperature and incubated overnight at 4 °C with primary antibody for Myc (CST, #13987S), PARP (CST, 9542T), cleaved-PARP (CST, D64E10), caspase-3 (CST D3R6Y), FBXW7 (ptglab, 28424-1-AP) phospho MYC T58 (CST, E4Z2K), phospho MYC S62 (CST, E1J4K), or β-actin (CST, #3700T). The membranes were then washed three times for 5 min each with PBST at room temperature. The blots were probed by horseradish peroxidase (HRP)-conjugated antirabbit or antimouse secondary antibody and detected by the chemiluminescent HRP substrate. Images of the blots were digitally visualized using an Imager and quantified with ImageJ software.

14. Cellular Thermal Shift Assay (CETSA). P493-6 cells were grown up to 70% confluence in the T75 flask. The grown cells were seeded at a density of 300,000 cells per well into 6-well plates. The cells were incubated at 37 °C, after which they were treated with designated MY05 concentrations for 2 h. Control cells were left untreated. Next, the cells were collected, pelleted, and washed with PBS. The cells were then resuspended in PBS, maintaining the compound treatment, and aliquoted into PCR tubes, with each tube designated a temperature point. Each tube was heated to its designated temperature for 3 min using a Bio-Rad thermocycler, after which the cells were cooled to room temperature in 3 min, followed by snap-freezing in liquid nitrogen. The cells were then subjected to three freeze−thaw cycles and centrifuged at 20,000*g* 4 °C for 20 min to pellet aggregated proteins. The soluble protein solutions were collected and boiled at 90 °C for 5 min with Laemmli buffer. SDS-PAGE of the lysates was run, followed by western blotting. The membranes were probed for MYC and β-actin as loading control using MYC and β-actin antibodies (Cell Signaling Technology). Images of the blots were digitally visualized using an Imager, and blots were quantified with ImageJ software.

https://doi.org/10.1021/acs.jmedchem.4c02556
J. Med. Chem. 2025, 68, 6233−6251

15. Co-Immunoprecipitation Assay. MDA-MB 468 and P493-6 cells were seeded at a density of 500,000 cells in T25 flasks. The cells were treated with 25 μM MY05 or DMSO for the indicated times. Cells were then collected and lysed in hypotonic buffer containing 0.5% Nonidet P-40, followed by centrifugation at 20,000*g* for 1 min. The cytoplasmic-soluble fraction was placed on ice, while the insoluble pellet was lysed using Active Motif complete lysis buffer following the manufacturer's protocol. The lysed nuclear fraction was then combined with the cytoplasmic fraction. 2 mg of protein from both fractions was incubated with MYC antibody (Cell Signaling Technology) overnight, followed by further incubation with prewashed protein A/G agarose beads (Santa Cruz) for 4 h at 4 °C. The samples were washed three times with hypotonic buffer, digested with Laemmli buffer, and boiled at 90 °C for 10 min. The samples were then analyzed by western blotting.

16. Cycloheximide (CHX) Chase Assay. P493-6 and MDA-MB 468 cells seeded at a density of 500,000 cells per well in 6-well plates were treated with 25 μM MY05 or DMSO for control for 3 h, followed by treatment with 50 μg/mL CHX at indicated times. Cells were collected after treatment, pelleted, and lysed. Lysates were analyzed by western blotting, and bands were quantified using ImageJ software and plotted using GraphPad Prism. The curve was fit with the one-phase decay exponential equation to determine the half-life of the protein.

17. Apoptosis Assay. P493-6 cells seeded at a density of 500,000 cells per well in 6-well plates were treated at indicated concentrations of MY05, 10058-F4, or DMSO control for 24 h. Post treatment, cells and media were collected and pelleted. Each sample group except for the negative control was stained with propidium iodide (PI) and FITC dyes in Annexin V buffer, while single stain controls were stained with either PI or FITC dye. The controls were used to set the voltage and fluorescence, and samples were analyzed by FACS at 20,000 events per sample.

18. Mammosphere Formation Assay. MDA-MB-468 and MCF-7 cells were plated in a low-attachment 24-well plate at 4000 cells per well and cultured in Mammocult media for 48 h for formation of mammosphere. The cultured cells were then treated with 25 μM MY05 for 5 days. Control wells were left untreated. Images of the mammosphere formed were taken for the control and treatment wells.

19. Real-Time Quantitative Polymerase Chain Reaction (RT-qPCR). MDA-MB 468 and P493-6 cells were seeded at 500,000 cells per well and cultured with or without MY05 (25 μM) for the indicated time point. Cells were lysed post treatment, and total RNA was extracted using TRIzol reagent (Thermo Fisher Scientific) following the manufacturer's protocol. Total RNA was quantified with a nanodrop spectrophotometer. Total RNA was reversed-transcribed into cDNA by the polymerase chain reaction (PCR). A 20 μL master mix of reverse transcription buffer, dNTP mix, random primers, multiscribe reverse transcriptase, and nuclease-free water was prepared according to the manufacturer's protocol (Applied Biosystems High-Capacity cDNA Reverse Transcription Kit). The master mix was combined with RNA solution in PCR tubes, sealed, and centrifuged briefly to eliminate bubbles. PCR was performed with a four-step setting at 25 °C for 10 min step 1, 37 °C for 120 min step 2, 85 °C for 5 min step 3, and 4 °C hold for step 4. qPCR was then carried out using respective forward and reverse primers of MYC target genes incubated with cDNA and Fast SYBR green mix following the manufacturer's protocol (Applied Biosystems). Relative mRNA expression was processed and expressed as $\Delta\Delta$CT, and a heat map plot was generated using GraphPad Prism.

20. Proximity Ligation Assay (PLA). MDA-MB 468 cells were plated in microscopy slides and allowed to adhere overnight. Cells were treated with or without MDA-MB 468 cells for 12 h, after which they were fixed by incubating in 4% paraformaldehyde for 15 min at room temperature and permeabilized in 0.5% Triton-X at 37 °C. The cells were then washed in PBS, blocked in buffer, and incubated with 1:500 MYC (D3N8F) and MAX (H-2 sc-8011) primary antibodies for 1 h. The proximity ligation assay protocol was followed as directed by the manufacturer using the Duolink kit (Sigma, DUO92101). Images were collected with a Nikon confocal microscope.

21. Bulk RNA Sequencing. MDA-MB 468 cells were seeded in T25 flasks and allowed to adhere, followed by treatment with 25 μM MY05 for treatment groups and untreated for control groups. The experiment was performed in triplicate, and cells were treated for 24 h. The cells were harvested, lysed, and total RNA isolated using TRIzol reagent (Invitrogen), following the manufacturer's protocol. Isolated RNA was subjected to quality control analysis using Nanodrop for the A_{260}/A_{280} ratio to determine purity and RNA concentration, with an A_{260}/A_{280} ratio of ~1.9 being considered acceptable. RNA samples were then sent to Novogene for RNA sequencing, where the RNA integrity, purity, and concentration were determined using an Agilent 5400 bioanalyzer with the RIN cutoff set at ~8.5. NEB library was then constructed, followed by a library quality control, sequencing, and then data quality control to filter out low-quality reads, reads whose bases cannot be determined, and reads with adapters. Sequencing was performed using an Illumina Novaseq X Plus (PE 150) based on sequencing by synthesis. Quantification and analysis of sequencing results were performed using indicated bioinformatics and statistical tools, pathway and enrichment analysis was performed using GO, KEGG, and Reactome databases, and plots were generated with SR Plot and GraphPad Prism.

22. Human c-Myc Transcription Factor Assay. P493-6 cells were seeded and treated with compounds MY01, MY04, and MY05 at the specified concentration for 24 h. The nuclear extracts of the various cells were performed by using a Nuclear Extract kit (Raybiotech, USA) by following the manufacturer's protocol. Oligonucleotide-coated 96-well plates were incubated with 100 μL of the prepared transcription factor binding reaction system (blank, positive control, specific competitor, nonspecific competitor, and nuclear extracts of cell treated with MY01) according to the manufacturer's protocol (Raybiotech, USA). Then, the mixture was incubated overnight. The solution was discarded and washed 4× with 300 μL of 1× Wash Buffer. 100 μL of the prepared c-Myc primary antibody was added to each well and incubated at room temperature for 1 h. Then, the solution was discarded and washed 4× with 300 μL of 1× Wash Buffer. 100 μL of the prepared HRP-conjugated secondary antibody was added to each well and incubated at room temperature for 1 h. Then, 100 μL of TMB One-Step substrate reagent was added to each well and incubated for 30 min in the dark. 50 μL of the Stop solution was added to each well, and absorbances were read at 450 nm.

For P493-6 cells treated with compounds MY04 and MY05 at the specified concentration for 24 h, the nuclear extracts were made using a Nuclear Extract kit (Signosis, USA) following the manufacturer's protocol. Oligonucleotide-coated 96-well plates were incubated with 100 μL of the prepared transcription factor binding reaction system (blank, positive control, specific competitor, nonspecific competitor, and nuclear extracts) according to the manufacturer's protocol (Active motif, USA) and then incubated for 1 h at room temperature while rocking. The solution was discarded and washed 4× with 200 μL of 1× Wash Buffer. 100 μL of the prepared c-Myc primary antibody was added to each well and incubated at room temperature for 1 h. Then, the solution was discarded and washed 4× with 200 μL of 1× Wash Buffer. 100 μL of the prepared HRP-conjugated secondary antibody was added to each well and incubated at room temperature for 1 h, followed by the wash process. Then, 100 μL of developing solution was added to each well and incubated for 10 min in the dark. 100 μL of the Stop solution was added to each well, and absorbances were read at 450 nm with a reference wavelength of 655 nm using a Biotek plate reader.

C. Standard Method for In Vivo Biological Studies. Six-week-old female athymic nude (Nu/J) mice were purchased from Jackson Laboratories and allowed to acclimatize for 2 weeks. Mice were housed five mice per cage in a well-ventilated temperature and humidity-controlled room at a 12 h light−dark cycle and monitored by the Division of Animal Resources (DLAR), University of Kentucky. **Ethics statement**: Animal care and experiments were carried out in accordance with NIH guidelines (NIH publication No. 85-23 Rev. 1985) and approved by the Institutional Animal Care and Use Committee (IACUC) of the University of Kentucky protocol (#2019-3183).

https://doi.org/10.1021/acs.jmedchem.4c02556
J. Med. Chem. 2025, 68, 6233−6251

23. In Vivo Studies. Six-week-old female Nu/J mice were quarantined for 2 weeks, after which they were inoculated with 2×10^6 MDA-MB 468 cells orthotopically at the mammary fat pad. Tumor volumes were monitored, and mice were treated with 10 mg/kg MY05 or DMSO (33.3%) and Kolliphor (66.7%) vehicle when tumor volumes were >50 mm^3. Injections were performed subcutaneously thrice a week until the endpoint. Tumor volume was measured using an external caliper, and the body weight of the animal was monitored and recorded. Mice were euthanized at the endpoint, and their tumors were excised.

24. Immunohistochemistry. The excised tumor was cut and fixed in 10% neutral buffered formalin (NBF) for 24 h at room temperature, after which tumor tissue was washed and NBF was replaced by 70% ethanol. Fixed samples were processed and imaged by the Biospecimen Procurement and Translational Pathology core, University of Kentucky. Tumor tissue was cleared in xylene and immersed in paraffin to be embedded. Appropriate slices of tissue were made and mounted on glass slides. Subsequently, the slices were deparaffinized and rehydrated. Then, the slices were processed to block endogenous peroxidase activity with 3% H_2O_2 solution in methanol and incubated with anti-MYC, K_i-67, or CC3. Slices on slides were then processed for staining, dehydrated, and imaged.

25. Western Blot. The excised tumor was homogenized with chilled buffer (50 mM Tris-HCl, pH 7.4, 150 mM NaCl, 10 mM NaF, 1 mM EDTA (pH 8), 1% NP-40, 1% Na-deoxycholate, and 0.1% SDS) containing protease and phosphatase inhibitors using a Dounce homogenizer. Homogenate was incubated on ice for 30 min and sonicated for 5 min at a 10 s burst/10 s pause cycle for complete lysis. Lysate was centrifuged at 10,000*g* for 20 min at 4 °C to pellet cell debris. The supernatant was transferred into a clean Eppendorf tube to which Laemmli buffer was added and incubated at 90 °C on a heat block for 5 min. Lysates were resolved by 4−20% sodium dodecyl sulfate-polyacrylamide gel electrophoresis (SDS-PAGE; 200 V for 35 min), followed by electro-transfer to a polyvinylidene difluoride membrane (PVDF, 100 V for 1 h). The membranes were blocked in 3% (w/v) bovine serum albumin (BSA) in PBST for 1 h at room temperature and incubated overnight at 4 °C with the primary antibody for Myc (CST, #13987S) or *β*-actin (CST, #3700T). The membranes were then washed three times for 5 min each with PBST at room temperature. The blots were probed by horseradish peroxidase (HRP)-conjugated antirabbit or antimouse secondary antibody and detected by the chemiluminescent HRP substrate. Images of the blots were digitally visualized using an Imager and quantified with ImageJ software.

■ ASSOCIATED CONTENT

Supporting Information

The Supporting Information is available free of charge at https://pubs.acs.org/doi/10.1021/acs.jmedchem.4c02556.

Characterization; ^1H and ^{13}C spectra; HPLC traces; APCI-MS; HPLC chromatogram of **MY01−07**; dose−response curves for **MY01−07** and 10058-F4; circular dichroism spectra; and supporting data for biological studies with MY05 (PDF)

Molecular formula strings (CSV)

■ AUTHOR INFORMATION

Corresponding Author

Samuel G. Awuah − *Department of Chemistry, University of Kentucky, Lexington, Kentucky 40506, United States; Center for Pharmaceutical Research and Innovation, Department of Pharmaceutical Sciences, College of Pharmacy and Markey NCI Comprehensive Cancer Center, University of Kentucky, Lexington, Kentucky 40536, United States; University of Kentucky Bioelectronics and Nanomedicine Research Center, Lexington, Kentucky 40506, United States;* orcid.org/0000-0003-4947-7283; Email: awuah@uky.edu

Authors

Oluwatosin A. Obisesan − *Department of Chemistry, University of Kentucky, Lexington, Kentucky 40506, United States;* orcid.org/0000-0001-6608-6765

Samuel Ofori − *Department of Chemistry, University of Kentucky, Lexington, Kentucky 40506, United States*

Owamagbe N. Orobator − *Department of Chemistry, University of Kentucky, Lexington, Kentucky 40506, United States*

Himanshi Sharma − *Department of Chemistry, University of Kentucky, Lexington, Kentucky 40506, United States*

Emma Groetecke − *Department of Chemistry, University of Kentucky, Lexington, Kentucky 40506, United States*

Complete contact information is available at: https://pubs.acs.org/10.1021/acs.jmedchem.4c02556

Notes

The authors declare the following competing financial interest(s): Samuel G. Awuah has patents pending to University of Kentucky Research Foundation. S.G.A. serves on the advisory board and is Chief Executive Officer of Ayarissa Biosciences.

■ ACKNOWLEDGMENTS

This work was supported by the National Science Foundation Chemistry of Life Processes (NSF-CLP) grant for S.G.A. (Award CHE-2203559). The authors would like to thank the following facilities at the University of Kentucky who provided support in completion of the experiments detailed in this manuscript. The UK NMR Center is supported by NSF (CHE-997738). This research was supported by the Cancer Research Informatics Shared Resource of the University of Kentucky Markey Cancer Center (P30CA177558). The authors also acknowledge the support of the Center for Pharmaceutical Research and Innovation (NIH P20GM130456). For the flow cytometry experiments, the authors thank UK Flow Cytometry, Pathology and Immune Function core supported by the Office of the Vice President of Research, Markey Cancer Center, and NCI Center Core Support Grant (P30 CA177558). The authors thank Prof. Giovanni Zinzalla at Karolinska Institutet (Stockholm, Sweden) for the MYC plasmid used. Thanks to Dr. Yadi Wu (University of Kentucky) and Dr. Anne Le (Johns Hopkins University) for the generous gifts of MCF-7 and P493-6 cells, respectively.

■ ABBREVIATIONS USED

AFDB, AlphaFold Data Bank; ANOVA, analysis of variance; aq, aqueous; ATP, adenosine triphosphate; b-HLH-LZ, basic helix−loop−helix leucine zipper; BSA, bovine serum albumin; cat, catalytic; CC3, cleaved caspase-3; CD, circular dichroism; cDNA, cDNA; CETSA, cellular thermal shift assay; DI, deionized; DMEM, Dulbecco's modified eagle medium; DMF, dimethylformamide; DMSO, dimethyl sulfoxide; DNA, deoxyribonucleic acid; ESI, electrospray ionization; EtOH, ethanol; FACS, fluorescence-activated cell sorting; FBS, fetal bovine serum; FITC, fluorescein isothiocyanate; GO, Gene Ontology; His-tag, histidine tag; HPLC, high-performance liquid chromatography; HRP, horseradish peroxidase; IC_{50}, half-maximum inhibitory concentration; IHC, immunohisto-

https://doi.org/10.1021/acs.jmedchem.4c02556
J. Med. Chem. 2025, 68, 6233−6251

chemistry; IPTG, isopropyl-L-thio-β-D-galactopyranoside; MeOH, methanol; MLAC, metal-mediated ligand affinity chemistry; MOE, molecular operating environment; MTT, 3-(4,5-dimethylthiazol-2-yl)-2,5-diphenyltetrazolium bromide; MW, molecular weight; ND, not determined; NMR, nuclear magnetic resonance; NTA, nitrilotriacetic; PAGE, polyacrylamide gel electrophoresis; PAINS, pan-assay interference compounds; PBS, phosphate buffer saline; PCR, polymerase chain reaction; PDB, Protein Data Bank; PI, propidium iodide; PONDR, predictor of natural disordered regions; Q1, quadrant 1; Q2, quadrant 2; Q3, quadrant 3; Q4, quadrant 4; qRT-PCR, quantitative real-time polymerase chain reaction; RP-HPLC, reverse-phase high-performance liquid chromatography; RPMI, Roswell Park memorial institute medium; SAR, structure−activity relationship; SD, standard deviation; SDS, sodium dodecyl sulfate; SEM, standard error mean; SI, selectivity index; THF, tetrahydrofuran; TNBC, triple-negative breast cancer

REFERENCES

(1) Conacci-Sorrell, M.; McFerrin, L.; Eisenman, R. N. An overview of MYC and its interactome. *Cold Spring Harbor Perspect. Med.* **2014**, *4* (1), No. a014357.

(2) Thomas, L. R.; Adams, C. M.; Wang, J.; Weissmiller, A. M.; Creighton, J.; Lorey, S. L.; Liu, Q.; Fesik, S. W.; Eischen, C. M.; Tansey, W. P. Interaction of the oncoprotein transcription factor MYC with its chromatin cofactor WDR5 is essential for tumor maintenance. *Proc. Natl. Acad. Sci. U.S.A.* **2019**, *116* (50), 25260−25268.

(3) Zhou, Y.; Gao, X.; Yuan, M.; Yang, B.; He, Q.; Cao, J. Targeting Myc Interacting Proteins as a Winding Path in Cancer Therapy. *Front. Pharmacol.* **2021**, *12*, No. 748852, DOI: 10.3389/fphar.2021.748852.

(4) Carroll, P. A.; Freie, B. W.; Mathsyaraja, H.; Eisenman, R. N. The MYC transcription factor network: balancing metabolism, proliferation and oncogenesis. *Front. Med.* **2018**, *12* (4), 412−425.

(5) Beaulieu, M. E.; Jauset, T.; Massó-Vallés, D.; Martínez-Martín, S.; Rahl, P.; Maltais, L.; Zacarias-Fluck, M. F.; Casacuberta-Serra, S.; Serrano Del Pozo, E.; Fiore, C.; et al. Intrinsic cell-penetrating activity propels Omomyc from proof of concept to viable anti-MYC therapy. *Sci. Transl Med.* **2019**, *11* (484), No. eaar5012, DOI: 10.1126/scitranslmed.aar5012.

(6) Dhanasekaran, R.; Deutzmann, A.; Mahauad-Fernandez, W. D.; Hansen, A. S.; Gouw, A. M.; Felsher, D. W. The MYC oncogene - the grand orchestrator of cancer growth and immune evasion. *Nat. Rev. Clin. Oncol.* **2022**, *19* (1), 23−36.

(7) Kalkat, M.; De Melo, J.; Hickman, K. A.; Lourenco, C.; Redel, C.; Resetca, D.; Tamachi, A.; Tu, W. B.; Penn, L. Z. MYC deregulation in primary human cancers. *Genes* **2017**, *8* (6), 151.

(8) Xu-Monette, Z. Y.; Deng, Q.; Manyam, G. C.; Tzankov, A.; Li, L.; Xia, Y.; Wang, X. X.; Zou, D.; Visco, C.; Dybkær, K.; et al. Clinical and Biologic Significance of MYC Genetic Mutations in De Novo Diffuse Large B-cell Lymphoma. *Clin. Cancer Res.* **2016**, *22* (14), 3593−3605.

(9) Han, H.; Jain, A. D.; Truica, M. I.; Izquierdo-Ferrer, J.; Anker, J. F.; Lysy, B.; Sagar, V.; Luan, Y.; Chalmers, Z. R.; Unno, K.; et al. Small-Molecule MYC Inhibitors Suppress Tumor Growth and Enhance Immunotherapy. *Cancer Cell* **2019**, *36* (5), 483−497.e415.

(10) Sammak, S.; Allen, M. D.; Hamdani, N.; Bycroft, M.; Zinzalla, G. The structure of INI1/hSNF5 RPT1 and its interactions with the c-MYC:MAX heterodimer provide insights into the interplay between MYC and the SWI/SNF chromatin remodeling complex. *FEBS J.* **2018**, *285* (22), 4165−4180.

(11) Napoli, C.; Lerman, L. O.; de Nigris, F.; Sica, V. c-Myc oncoprotein: a dual pathogenic role in neoplasia and cardiovascular diseases? *Neoplasia* **2002**, *4* (3), 185−190.

(12) Oster, S. K.; Mao, D. Y. L.; Kennedy, J.; Penn, L. Z. Functional analysis of the N-terminal domain of the Myc oncoprotein. *Oncogene* **2003**, *22* (13), 1998−2010.

(13) Das, S. K.; Lewis, B. A.; Levens, D. MYC: a complex problem. *Trends Cell Biol.* **2023**, *33* (3), 235−246.

(14) Sammak, S.; Hamdani, N.; Gorrec, F.; Allen, M. D.; Freund, S. M. V.; Bycroft, M.; Zinzalla, G. Crystal Structures and Nuclear Magnetic Resonance Studies of the Apo Form of the c-MYC:MAX bHLHZip Complex Reveal a Helical Basic Region in the Absence of DNA. *Biochemistry* **2019**, *58* (29), 3144−3154.

(15) Beaulieu, M. E.; Castillo, F.; Soucek, L. Structural and Biophysical Insights into the Function of the Intrinsically Disordered Myc Oncoprotein. *Cells* **2020**, *9* (41038.

(16) Blackwood, E. M.; Eisenman, R. N. Max: a helix-loop-helix zipper protein that forms a sequence-specific DNA-binding complex with Myc. *Science* **1991**, *251* (4998), 1211−1217.

(17) Zhou, Y.; Gao, X.; Yuan, M.; Yang, B.; He, Q.; Cao, J. Targeting Myc Interacting Proteins as a Winding Path in Cancer Therapy. *Front. Pharmacol.* **2021**, *12*, No. 748852.

(18) Beaulieu, M.-E.; Castillo, F.; Soucek, L. Structural and Biophysical Insights into the Function of the Intrinsically Disordered Myc Oncoprotein. *Cells* **2020**, *9* (4), 1038.

(19) Farina, A.; Faiola, F.; Martinez, E. Reconstitution of an E box-binding Myc:Max complex with recombinant full-length proteins expressed in *Escherichia coli*. *Protein Expr. Purif.* **2004**, *34* (2), 215−222.

(20) Amati, B.; Brooks, M. W.; Levy, N.; Littlewood, T. D.; Evan, G. I.; Land, H. Oncogenic activity of the c-Myc protein requires dimerization with Max. *Cell* **1993**, *72* (2), 233−245.

(21) Lin, C. Y.; Lovén, J.; Rahl, P. B.; Paranal, R. M.; Burge, C. B.; Bradner, J. E.; Lee, T. I.; Young, R. A. Transcriptional Amplification in Tumor Cells with Elevated c-Myc. *Cell* **2012**, *151* (1), 56−67.

(22) Schulze, A.; Oshi, M.; Endo, I.; Takabe, K. MYC Targets Scores Are Associated with Cancer Aggressiveness and Poor Survival in ER-Positive Primary and Metastatic Breast Cancer. *Int. J. Mol. Sci.* **2020**, *21* (218127.

(23) Meškytė, E. M.; Keskas, S.; Ciribilli, Y. MYC as a Multifaceted Regulator of Tumor Microenvironment Leading to Metastasis. *Int. J. Mol. Sci.* **2020**, *21* (207710.

(24) Doha, Z. O.; Wang, X.; Calistri, N. L.; Eng, J.; Daniel, C. J.; Ternes, L.; Kim, E. N.; Pelz, C.; Munks, M.; Betts, C.; et al. MYC Deregulation and PTEN Loss Model Tumor and Stromal Heterogeneity of Aggressive Triple-Negative Breast Cancer. *Nat. Commun.* **2023**, *14* (1), No. 5665.

(25) Chen, H.; Liu, H.; Qing, G. Targeting oncogenic Myc as a strategy for cancer treatment. *Signal Transduction Targeted Ther.* **2018**, *3* (1), No. 5.

(26) Dang, C. V. MYC on the path to cancer. *Cell* **2012**, *149* (1), 22−35.

(27) Gabay, M.; Li, Y.; Felsher, D. W. MYC activation is a hallmark of cancer initiation and maintenance. *Cold Spring Harbor Perspect. Med.* **2014**, *4* (6), No. a014241, DOI: 10.1101/cshperspect.a014241.

(28) Wang, C.; Zhang, J.; Yin, J.; Gan, Y.; Xu, S.; Gu, Y.; Huang, W. Alternative approaches to target Myc for cancer treatment. *Signal Transduction Targeted Ther.* **2021**, *6* (1), No. 117.

(29) Duffy, M. J.; O'Grady, S.; Tang, M.; Crown, J. MYC as a target for cancer treatment. *Cancer Treatment Reviews* **2021**, *94*, No. 102154.

(30) Choi, S. H.; Mahankali, M.; Lee, S. J.; Hull, M.; Petrassi, H. M.; Chatterjee, A. K.; Schultz, P. G.; Jones, K. A.; Shen, W. Targeted disruption of Myc−Max oncoprotein complex by a small molecule. *ACS Chem. Biol.* **2017**, *12* (11), 2715−2719.

(31) Lu, X.; Vogt, P. K.; Boger, D. L.; Lunec, J. Disruption of the MYC transcriptional function by a small-molecule antagonist of MYC/MAX dimerization. *Oncol. Rep.* **2008**, *19* (3), 825−830.

(32) Berg, T.; Cohen, S. B.; Desharnais, J.; Sonderegger, C.; Maslyar, D. J.; Goldberg, J.; Boger, D. L.; Vogt, P. K. Small-molecule antagonists of Myc/Max dimerization inhibit Myc-induced transformation of chicken embryo fibroblasts. *Proc. Natl. Acad. Sci. U.S.A.* **2002**, *99* (6), 3830−3835.

https://doi.org/10.1021/acs.jmedchem.4c02556
J. Med. Chem. 2025, 68, 6233−6251

(33) Hammoudeh, D. I.; Follis, A. V.; Prochownik, E. V.; Metallo, S. J. Multiple Independent Binding Sites for Small-Molecule Inhibitors on the Oncoprotein c-Myc. *J. Am. Chem. Soc.* **2009**, *131* (21), 7390−7401.
(34) Yin, X.; Giap, C.; Lazo, J. S.; Prochownik, E. V. Low molecular weight inhibitors of Myc−Max interaction and function. *Oncogene* **2003**, *22* (40), 6151−6159.
(35) Whitfield, J. R.; Beaulieu, M.-E.; Soucek, L. Strategies to inhibit Myc and their clinical applicability. *Front. Cell Dev. Biol.* **2017**, *5*, 10.
(36) Wang, H.; Hammoudeh, D. I.; Follis, A. V.; Reese, B. E.; Lazo, J. S.; Metallo, S. J.; Prochownik, E. V. Improved low molecular weight Myc-Max inhibitors. *Mol. Cancer Ther.* **2007**, *6* (9), 2399−2408.
(37) Kumar, D.; Sharma, N.; Giri, R. Therapeutic Interventions of Cancers Using Intrinsically Disordered Proteins as Drug Targets: c-Myc as Model System. *Cancer Inf.* **2017**, *16*, No. 1176935117699408.
(38) Yu, C.; Niu, X.; Jin, F.; Liu, Z.; Jin, C.; Lai, L. Structure-based Inhibitor Design for the Intrinsically Disordered Protein c-Myc. *Sci. Rep.* **2016**, *6* (1), No. 22298.
(39) Madden, S. K.; de Araujo, A. D.; Gerhardt, M.; Fairlie, D. P.; Mason, J. M. Taking the Myc out of cancer: toward therapeutic strategies to directly inhibit c-Myc. *Mol. Cancer* **2021**, *20* (1), No. 3.
(40) Meng, Q.; Xia, Y. c-Jun, at the crossroad of the signaling network. *Protein Cell* **2011**, *2* (11), 889−898.
(41) Whitfield, J. R.; Soucek, L. The long journey to bring a Myc inhibitor to the clinic. *J. Cell Biol.* **2021**, *220* (8), No. e202103090, DOI: 10.1083/jcb.202103090.
(42) Demma, M. J.; Mapelli, C.; Sun, A.; Bodea, S.; Ruprecht, B.; Javaid, S.; Wiswell, D.; Muise, E.; Chen, S.; Zelina, J.; et al. Omomyc Reveals New Mechanisms To Inhibit the MYC Oncogene. *Mol. Cell. Biol.* **2019**, *39* (22), No. e00248-19, DOI: 10.1128/MCB.00248-19.
(43) Direct MYC Inhibitor Passes First Clinical Test. *Cancer Discovery* **2023**, *131* 4. DOI: 10.1158/2159-8290.Cd-nb2022-0067.
(44) Mullard, A. Climbing cancer's MYC mountain. *Nat. Rev. Drug Discovery* **2022**, *21* (12), 865−867.
(45) Singh, A.; Kumar, P.; Sarvagalla, S.; Bharadwaj, T.; Nayak, N.; Coumar, M. S.; Giri, R.; Garg, N. Functional inhibition of c-Myc using novel inhibitors identified through "hot spot" targeting. *J. Biol. Chem.* **2022**, *298* (5), No. 101898.
(46) Li, Z.; Huang, Y.; Hung, T. I.; Sun, J.; Aispuro, D.; Chen, B.; Guevara, N.; Ji, F.; Cong, X.; Zhu, L.; et al. MYC-Targeting Inhibitors Generated from a Stereodiversified Bicyclic Peptide Library. *J. Am. Chem. Soc.* **2024**, *146* (2), 1356−1363.
(47) Gukathasan, S.; Parkin, S.; Black, E. P.; Awuah, S. G. Tuning Cyclometalated Gold(III) for Cysteine Arylation and Ligand-Directed Bioconjugation. *Inorg. Chem.* **2021**, *60* (19), 14582−14593.
(48) Ofori, S.; Gukathasan, S.; Awuah, S. G. Gold-Based Pharmacophore Inhibits Intracellular MYC Protein. *Chem. − Eur. J.* **2021**, *27* (12), 4168−4175.
(49) Irwin, J. J.; Sterling, T.; Mysinger, M. M.; Bolstad, E. S.; Coleman, R. G. ZINC: A Free Tool to Discover Chemistry for Biology. *J. Chem. Inf. Model.* **2012**, *52* (7), 1757−1768.
(50) Vilar, S.; Cozza, G.; Moro, S. Medicinal chemistry and the molecular operating environment (MOE): application of QSAR and molecular docking to drug discovery. *Curr. Top Med. Chem.* **2008**, *8* (18), 1555−1572.
(51) Horiuchi, D.; Anderton, B.; Goga, A. Taking on challenging targets: making MYC druggable. *Am. Soc. Clin. Oncol. Educ. Book* **2014**, e497−e502.
(52) Nair, S. K.; Burley, S. K. X-Ray Structures of Myc-Max and Mad-Max Recognizing DNA: Molecular Bases of Regulation by Proto-Oncogenic Transcription Factors. *Cell* **2003**, *112* (2), 193−205.
(53) Varadi, M.; Anyango, S.; Deshpande, M.; Nair, S.; Natassia, C.; Yordanova, G.; Yuan, D.; Stroe, O.; Wood, G.; Laydon, A.; et al. AlphaFold Protein Structure Database: massively expanding the structural coverage of protein-sequence space with high-accuracy models. *Nucleic Acids Res.* **2022**, *50* (D1), D439−D444.
(54) Varadi, M.; Bertoni, D.; Magana, P.; Paramval, U.; Pidruchna, I.; Radhakrishnan, M.; Tsenkov, M.; Nair, S.; Mirdita, M.; Yeo, J.; et al. AlphaFold Protein Structure Database in 2024: providing structure coverage for over 214 million protein sequences. *Nucleic Acids Res.* **2024**, *52* (D1), D368−D375.
(55) Kiessling, A.; Sperl, B.; Hollis, A.; Eick, D.; Berg, T. Selective inhibition of c-Myc/Max dimerization and DNA binding by small molecules. *Chem. Biol.* **2006**, *13* (7), 745−751.
(56) Michel, J.; Cuchillo, R. The impact of small molecule binding on the energy landscape of the intrinsically disordered protein C-myc. *PLoS One* **2012**, *7* (7), No. e41070.
(57) Müller, I.; Larsson, K.; Frenzel, A.; Oliynyk, G.; Zirath, H.; Prochownik, E. V.; Westwood, N. J.; Henriksson, M. A. Targeting of the MYCN protein with small molecule c-MYC inhibitors. *PLoS One* **2014**, *9* (5), No. e97285.
(58) Heller, G. T.; Aprile, F. A.; Bonomi, M.; Camilloni, C.; De Simone, A.; Vendruscolo, M. Sequence Specificity in the Entropy-Driven Binding of a Small Molecule and a Disordered Peptide. *J. Mol. Biol.* **2017**, *429* (18), 2772−2779.
(59) Follis, A. V.; Hammoudeh, D. I.; Wang, H.; Prochownik, E. V.; Metallo, S. J. Structural rationale for the coupled binding and unfolding of the c-Myc oncoprotein by small molecules. *Chem. Biol.* **2008**, *15* (11), 1149−1155.
(60) Fladvad, M.; Zhou, K.; Moshref, A.; Pursglove, S.; Säfsten, P.; Sunnerhagen, M. N and C-terminal Sub-regions in the c-Myc Transactivation Region and their Joint Role in Creating Versatility in Folding and Binding. *J. Mol. Biol.* **2005**, *346* (1), 175−189.
(61) Huang, M. J.; Cheng, Y. C.; Liu, C. R.; Lin, S.; Liu, H. E. A small-molecule c-Myc inhibitor, 10058-F4, induces cell-cycle arrest, apoptosis, and myeloid differentiation of human acute myeloid leukemia. *Exp. Hematol.* **2006**, *34* (11), 1480−1489.
(62) Xu, J.; Chen, Y.; Olopade, O. I. MYC and Breast Cancer. *Genes Cancer* **2010**, *1* (6), 629−640.
(63) Kang, J.; Sergio, C. M.; Sutherland, R. L.; Musgrove, E. A. Targeting cyclin-dependent kinase 1 (CDK1) but not CDK4/6 or CDK2 is selectively lethal to MYC-dependent human breast cancer cells. *BMC Cancer* **2014**, *14* (1), No. 32.
(64) Schuhmacher, M.; Staege, M. S.; Pajic, A.; Polack, A.; Weidle, U. H.; Bornkamm, G. W.; Eick, D.; Kohlhuber, F. Control of cell growth by c-Myc in the absence of cell division. *Curr. Biol.* **1999**, *9* (21), 1255−1258.
(65) Pajic, A.; Spitkovsky, D.; Christoph, B.; Kempkes, B.; Schuhmacher, M.; Staege, M. S.; Brielmeier, M.; Ellwart, J.; Kohlhuber, F.; Bornkamm, G. W.; et al. Cell cycle activation by c-myc in a burkitt lymphoma model cell line. *Int. J. Cancer* **2000**, *87* (6), 787−793.
(66) Wang, C.; Mayer, J. A.; Mazumdar, A.; Fertuck, K.; Kim, H.; Brown, M.; Brown, P. H. Estrogen Induces c-myc Gene Expression via an Upstream Enhancer Activated by the Estrogen Receptor and the AP-1 Transcription Factor. *Mol. Endocrinol.* **2011**, *25* (9), 1527−1538.
(67) Xue, B.; Dunbrack, R. L.; Williams, R. W.; Dunker, A. K.; Uversky, V. N. PONDR-FIT: a meta-predictor of intrinsically disordered amino acids. *Biochim. Biophys. Acta, Proteins Proteomics* **2010**, *1804* (4), 996−1010.
(68) Greenfield, N. J. Analysis of the kinetics of folding of proteins and peptides using circular dichroism. *Nat. Protoc.* **2006**, *1* (6), 2891−2899.
(69) Greenfield, N. J. Using circular dichroism collected as a function of temperature to determine the thermodynamics of protein unfolding and binding interactions. *Nat. Protoc.* **2006**, *1* (6), 2527−2535.
(70) Huynh, K.; Partch, C. L. Analysis of protein stability and ligand interactions by thermal shift assay. *Curr. Protoc Protein Sci.* **2015**, *79*, 28.29.21−28.29.14.
(71) Cimmperman, P.; Baranauskiene, L.; Jachimoviciūte, S.; Jachno, J.; Torresan, J.; Michailoviene, V.; Matuliene, J.; Sereikaite, J.; Bumelis, V.; Matulis, D. A quantitative model of thermal stabilization and destabilization of proteins by ligands. *Biophys. J.* **2008**, *95* (7), 3222−3231.

(72) Jafari, R.; Almqvist, H.; Axelsson, H.; Ignatushchenko, M.; Lundbäck, T.; Nordlund, P.; Molina, D. M. The cellular thermal shift assay for evaluating drug target interactions in cells. *Nat. Protoc.* **2014**, *9* (9), 2100−2122.
(73) Tolvanen, T. A. Current Advances in CETSA. *Front. Mol. Biosci.* **2022**, *9*, No. 866764, DOI: 10.3389/fmolb.2022.866764.
(74) Sanchez, T. W.; Ronzetti, M. H.; Owens, A. E.; Antony, M.; Voss, T.; Wallgren, E.; Talley, D.; Balakrishnan, K.; Leyes Porello, S. E.; Rai, G.; et al. Real-Time Cellular Thermal Shift Assay to Monitor Target Engagement. *ACS Chem. Biol.* **2022**, *17* (9), 2471−2482.
(75) Wang, X.; Cunningham, M.; Zhang, X.; Tokarz, S.; Laraway, B.; Troxell, M.; Sears, R. C. Phosphorylation regulates c-Myc's oncogenic activity in the mammary gland. *Cancer Res.* **2011**, *71* (3), 925−936.
(76) Chen, G. S.; Chen, S. Y.; Liu, S. T.; Hsieh, C. C.; Lee, S. P.; Huang, S. M. Stabilization of the c-Myc Protein via the Modulation of Threonine 58 and Serine 62 Phosphorylation by the Disulfiram/Copper Complex in Oral Cancer Cells. *Int. J. Mol. Sci.* **2022**, *23* (16), 9137 DOI: 10.3390/ijms23169137.
(77) Wang, X.; Langer, E. M.; Daniel, C. J.; Janghorban, M.; Wu, V.; Wang, X.-J.; Sears, R. C. Altering MYC phosphorylation in the epidermis increases the stem cell population and contributes to the development, progression, and metastasis of squamous cell carcinoma. *Oncogenesis* **2020**, *9* (9), No. 79.
(78) Wasylishen, A. R.; Chan-Seng-Yue, M.; Bros, C.; Dingar, D.; Tu, W. B.; Kalkat, M.; Chan, P.-K.; Mullen, P. J.; Huang, L.; Meyer, N.; et al. MYC Phosphorylation at Novel Regulatory Regions Suppresses Transforming Activity. *Cancer Res.* **2013**, *73* (21), 6504−6515.
(79) Ward, T. H.; Cummings, J.; Dean, E.; Greystoke, A.; Hou, J. M.; Backen, A.; Ranson, M.; Dive, C. Biomarkers of apoptosis. *Br. J. Cancer* **2008**, *99* (6), 841−846.
(80) Pinto, B.; Henriques, A. C.; Silva, P. M. A.; Bousbaa, H. Three-Dimensional Spheroids as In Vitro Preclinical Models for Cancer Research. *Pharmaceutics* **2020**, *12* (121186.
(81) Donati, G.; Amati, B. MYC and therapy resistance in cancer: risks and opportunities. *Mol. Oncol.* **2022**, *16* (21), 3828−3854.
(82) Wang, H.; Chauhan, J.; Hu, A.; Pendleton, K.; Yap, J. L.; Sabato, P. E.; Jones, J. W.; Perri, M.; Yu, J.; Cione, E.; et al. Disruption of Myc-Max heterodimerization with improved cell-penetrating analogs of the small molecule 10074-G5. *Oncotarget* **2013**, *4* (6), 936−947.
(83) Singh, A.; Kumar, A.; Kumar, P.; Nayak, N.; Bhardwaj, T.; Giri, R.; Garg, N. A novel inhibitor L755507 efficiently blocks c-Myc−MAX heterodimerization and induces apoptosis in cancer cells. *J. Biol. Chem.* **2021**, *297* (1), No. 100903.
(84) Oei, V.; Chuang, L. S. H.; Matsuo, J.; Srivastava, S.; Teh, M.; Ito, Y. RUNX3 inactivates oncogenic MYC through disruption of MYC/MAX complex and subsequent recruitment of GSK3β-FBXW7 cascade. *Commun. Biol.* **2023**, *6* (1), No. 689.
(85) Wang, H.; Teriete, P.; Hu, A.; Raveendra-Panickar, D.; Pendelton, K.; Lazo, J. S.; Eiseman, J.; Holien, T.; Misund, K.; Oliynyk, G.; et al. Direct inhibition of c-Myc-Max heterodimers by celastrol and celastrol-inspired triterpenoids. *Oncotarget* **2015**, *6* (32), 32380−32395, DOI: 10.18632/oncotarget.6116.
(86) Celej, M. S.; Montich, G. G.; Fidelio, G. D. Protein stability induced by ligand binding correlates with changes in protein flexibility. *Protein Sci.* **2003**, *12* (7), 1496−1506.
(87) McCammon, M. G.; Robinson, C. V. Structural change in response to ligand binding. *Curr. Opin. Chem. Biol.* **2004**, *8* (1), 60−65.
(88) Weber, L. I.; Hartl, M. Strategies to target the cancer driver MYC in tumor cells. *Front. Oncol* **2023**, *13*, No. 1142111.
(89) Beaulieu, M.-E.; Jauset, T.; Massó-Vallés, D.; Martínez-Martín, S.; Rahl, P.; Maltais, L.; Zacarias-Fluck, M. F.; Casacuberta-Serra, S.; Serrano del Pozo, E.; Fiore, C.; et al. Intrinsic cell-penetrating activity propels Omomyc from proof of concept to viable anti-MYC therapy. *Sci. Transl. Med.* **2019**, *11* (484), No. eaar5012.
(90) Garralda, E.; Beaulieu, M.-E.; Moreno, V.; Casacuberta-Serra, S.; Martínez-Martín, S.; Foradada, L.; Alonso, G.; Massó-Vallés, D.; López-Estévez, S.; Jauset, T.; et al. MYC targeting by OMO-103 in solid tumors: a phase 1 trial. *Nat. Med.* **2024**, *30* (3), 762−771.

https://doi.org/10.1021/acs.jmedchem.4c02556
J. Med. Chem. 2025, 68, 6233−6251